Analysis of electrophysiological data

Michael Pusch

Istituto di Biofisica, Consiglio Nazionale delle Ricerche, Via de Marini 6, I-16149 Genova, Italy, phone: 39-0106475-561; fax: 39-0106475-500; e-mail: pusch@ge.ibf.cnr.it.

1. Overview

In this chapter I will explain electrophysiological methods to extract biophysical parameters that allow a characterization of the two fundamental properties of ion channels: gating and permeation. The Introduction provides a broad overview of the general concepts of ion channel biophysics. The later chapters introduce several concrete methods for the analysis of electrophysiological experiments on heterologously expressed ion channels. The text provides an overview about the kind of information that can be extracted from electrophysiological recordings. Many parts are explicit and can be directly applied "at the bench" (or better say at the setup). Other, more advanced topics (gating current measurements, single-channel kinetic analysis) are touched more superficially. Their application requires further background that can be found in the references.
I include several mathematical equations. Most of them are simple and of direct practical value. I think it is useful to become familiar with a concrete and quantitative approach, in order to be able to design, execute, and analyze electrophysiological experiments. Readers interested in the theoretical background of most of the concepts outlined in this chapter are referred to [1] and references therein.

2. Introduction

The function of ion channels is to pass – in a passive but selective manner – in a short time a large number of ions across biological membranes. This electrogenicity is exploited by excitable cells to quickly change the transmembrane voltage allowing for example the traveling action potential and the postsynaptic electrical response to chemical neurotransmission. Other cells and organelles exploit the large capacity of charge transport for ion homeostasis and transepithelial transport. For the researcher the electrogenicity is handy because it allows the measurement of ion channel functioning in "real-time". It is possible to monitor the action of ion channels *in vivo* or in appropriate

simplified *in vitro* systems like brain slices. Intracellular electrodes directly measure the membrane voltage of individual cells while extracellular electrodes monitor indirectly the electrical activity of several cells. However, the recording of the physiological voltage does not tell much about the biophysical parameters of the underlying channels for two main reasons. First, all cells possess a mixture of different ion channels and other electrogenic transporters making it difficult to tease apart their respective contribution to the electrical response. Second, the physiological recordings are current-clamp measurements in which the membrane voltage is "freely floating". Similarly, the concentration of neurotransmitters or other ligands is uncontrolled in such physiological experiments. However, physically speaking, the membrane voltage and the concentration of a ligand are intensive variables, that is they do not depend on the size of the system and they can be directly "sensed" by an appropriate device. In order to reliably define a physical parameter of an ion channel (ligand affinity, slope of the voltage-dependence, …) the intensive variables have to be fixed, or "clamped". A further important step is to isolate as much as possible a single type of ion channel. In physiological preparations this can be partially achieved using appropriate solutions and blocking agents. Heterologous systems are even better in this respect, even if they carry the risk that some physiologically important molecular component is missing.

From the perspective described above the application and interpretation of the voltage-clamp measurements by Hodgkin and Huxley [2] have revolutionized the approach of ion channel study and also today's description and interpretation of ion channel function is still formulated in the same spirit. One of the most important concepts for ion channels is the "gate". A gate can be either open or shut (closed). There is no intermediate, half-open gate. At the time of Hodgkin and Huxley this was almost mere speculation as practically nothing was known at the level of single channels. But the assumption of a simple open or closed gate allowed a convenient description as a two-state Markov process associated

with a linear differential equation at a fixed voltage or ligand concentration. For the classical "m-gate", the activation gate of the voltage-gated Na^+ channel, this equation reads

$$\frac{dm}{dt}(t) = -\beta m(t) + \alpha(1 - m(t))$$

where "*m(t)*" is the probability of the gate to be open at time *t*. The opening and closing rate constants, α and β, respectively, are voltage-dependent and represent a model for the underlying molecular rearrangement leading to gate opening. A verification of the open-closed dichotomy of most ion channels became possible with the patch clamp technique [3,4] that allowed the real-time visualization of single channel opening and closing in almost all types of existing animal, plant, and bacterial cells (for the sake of clarity, I am neglecting here the existence of "subconductance" states, "flickering", and other probably ubiquitous complicated single-channel behavior). Of course, the description of gating as a two-state process is an idealization. Opening is not instantaneous but it takes a finite time to convert a closed to an open channel. Also, microscopically, there does not exist something like a single "open" state, but rather an almost infinite number of possible molecular configurations, that are macroscopically lumped together into "the open" state, because functionally, they are almost indistinguishable from each other. The transitions from closed to open (and vice-versa) appear "instantaneously" on single channel recordings. Thus they take place in less than, let's say, about 1 µs. However, despite the availability of several ion channel structures (for example [5-7]) and large computing power it is not yet possible to explore channel gating by molecular dynamics. Even ion permeation, that occurs on a much faster time scale, can not be fully simulated even though some theoretical progress has been made especially for K^+ channels (see for example [8]). Quantitative functional measurements are still essential for a detailed insight into the mechanisms of ion channels. It can be expected that many more structural data

for ion channels will be available in the near future. The structures will guide computational studies and rational mutagenesis in order to understand mechanisms of function at a molecular model, to obtain high affinity ligands, and possibly to exploit ion channels as molecular devices in applied technological systems. Computational predictions and structure based hypotheses have to be tested experimentally with functional data. The present chapter wants to provide an aid in designing, analyzing and interpreting such measurements.

3. Expression systems and related recording techniques

Each type of heterologous expression system determines a range of possible recording techniques. The most popular expression systems are *Xenopus* oocytes and mammalian cell lines, like HEK293 or CHO cells. A more rarely used system is the incorporation of relatively crude vesicles or purified proteins into planar lipid bilayers.

3.1 Expression in *Xenopus* oocytes

The expression in *Xenopus* oocytes represents an extremely versatile system that allows the application of many different electrophysiological and also biochemical methods [9-11]. Normally, *in vitro* transcribed cRNA is microinjected but expression can also be achieved using nuclear injection of eukaryotic expression plasmids. The oocyte system is so popular because electrophysiological recordings can be quite easily performed also by non-experts employing the two-electrode voltage-clamp technique (TEV) [9]. This method allows a relatively high throughput compared to patch clamp techniques and is thus often used for example for drug screening. A commonly underestimated problem of the TEV technique that is relevant also for qualitative measurements concerns the error introduced by the so-called series resistance (see for example [12]). The series resistance is caused by a finite conductivity of the oocyte cytoplasm, leading to a voltage drop within the

cytoplasm and thus to a voltage error (see Fig. 1). Typical values of the series resistance are in the order of 0.5 - 1 kΩ. Thus a current of 10 µA will cause a voltage error of the order of 5-10 mV, a value that can often not be neglected.

[PLACE HERE FIGURE 1]

Furthermore, even when the series resistance is taken into account, as is possible using recent standard equipment, the TEV technique has a quite limited time resolution of the order of almost 1 ms in most real-world applications. The apparent time resolution can be boosted with special tricks but the oocyte nevertheless provides an non-ideal space-clamp. "Fast" kinetic parameters that are derived from TEV measurements are therefore seldom comparable to the same parameters measured with the patch clamp technique. Another disadvantage of whole oocytes is that their cytoplasmic content can not be controlled. This may lead to a significant variability of measurements from different oocytes if the channel properties depend on the cytosolic composition. Also one often would like to change or at least to fix the intracellular solution. Furthermore, in the case of large expression the intracellular ion concentrations can be significantly altered by the voltage-clamp measurements. For example it is very difficult to handle a large expression (> 10 µA) of the Cl^- selective muscle channel CLC-1, because its kinetics strongly depends on the intracellular Cl^- concentration.

The disadvantages described above are partially overcome by the "cut-open" oocyte technique [13]. With this method only a small part of the surface area of the oocyte is clamped and the intracellular solution can be exchanged. However, the method is low throughput, necessitates quite a bit of skill, and perfusion of the interior solution is very slow. Thus, this method is likely to be applied only for special applications.

A general problem with the expression of Ca^{2+}-permeable channels or channels that depend on intracellular Ca^{2+} is that *Xenopus* oocytes endogenously express a quite large Ca^{2+} dependent Cl^- current, $I_{Cl\text{-}}(Ca^{2+})$ [14,15]. With maximal stimulation $I_{Cl\text{-}}(Ca^{2+})$ can reach several tens of µA of current. Thus activation of Ca^{2+} permeable channels that leads to an influx of Ca^{2+} will inevitably activate this endogenous current and confound the measurements. It is also practically impossible to manipulate the intracellular Ca^{2+} concentration in order to study its effect on expressed channels. However, the endogenous current can be exploited as a Ca^{2+} sensor to test for a possible Ca^{2+} permeability and also to test if the activation of (expressed) receptors and/or G-proteins results in an increase of the intracellular Ca^{2+} concentration (see for example [16]).

After highlighting the disadvantages of the oocytes system it is necessary to not forget that, in addition to its ease of use, it presents several significant advantages relative to other systems. One of these is that several cRNA's coding for different subunits of an ion channel or other interacting proteins can be co-injected at defined proportions. For example dominant heterozygous genotypes of channelopathies can be simulated by a one to one co-expression of WT and mutant subunits, and possible dominant negative effects can be quantified (see for example [17]). Co-expression of different proteins can also be achieved in transfected cells. However, with the oocyte injection it is easier to precisely control the relative expression of each protein.

Another advantage is that within one and the same oocyte the electrical activity recorded with the TEV can be correlated with the surface expression of the expressed protein using for example an introduced extracellular epitope [18,19]. This is of particular importance for channelopathies because many disease causing mutations are pathogenic because they effectively reduce or enhance the plasma membrane expression of the channel (see for example [18,20]).

Also the patch clamp technique can be applied to *Xenopus* oocytes after the vitelline membrane has been removed [10]. Recordings can be performed in the cell-attached, the inside out and the outside out configuration (see [4] for a description of these methods). The electrical properties of the obtainable seal are exceptional with seal resistances > 100 GΩ being possible allowing very high resolution recordings. The size of the patch pipette can be from very small to "giant" [21] allowing single-channel or macroscopic recordings. Rapid solution exchanges can be applied to excised patches allowing a precise investigation of for example transmitter activated channels (see for example [22]). The good electrical properties of the cell-free patch clamp configuration represent a significant advantage over whole cell recordings of small cells that have a limited time-resolution due to the access (series) resistance (see below).

3.2 Expression in mammalian cells

Another popular expression system are "transfected" mammalian cell lines like HEK, CHO or many others [23]. The expression of one or more proteins is induced by the introduction of the DNA in an appropriate eukaryotic (often mammalian) expression vector by various chemical of physical methods. Cells can be either transiently or stably transfected. Stable transfection generally requires the integration of one or more copies of the expression construct into the genome and is thus initially much more labor intensive than transient transfection. It is, however, convenient if one and the same kind of channel shall be studied in a very detailed manner or for drug screening. Many molecular biological methods exist that increase transfection efficiency and the level of expression. Expression can also be induced with several different kinds of viruses [24].

The method of choice to study the function of channels expressed in these small cells is the patch clamp technique. All configurations (cell attached, whole cell, inside out, outside out) can be applied. The whole cell configuration is probably the one that is mostly used,

for example for drug screening. Indeed, several different technical approaches have been recently designed to automate the whole cell patch clamp for high throughput drug screening [25]. Several factors have to be considered for the analysis of whole cell data. The time resolution in voltage-jump experiments is limited by the time that is necessary to charge the membrane capacity, C_m, across the access resistance, R_a, and is thus given by

$$\tau = C_m R_a$$

Typical values of C_m = 20 pF, R_a = 5 MΩ, yield a charging time constant of 0.1 ms. This is sufficient for most applications but can lead to problems for very fast kinetics observed for example in voltage-gated Na^+ or Cl^- channels [26,27].

The access resistance leads also to an error of the voltage-reading similar to the series resistance problem in the two-electrode voltage-clamp. For a membrane current I_m the voltage error amounts to

$$\Delta V = I_m R_a$$

which for typical values R_a = 5 MΩ, I_m = 1 nA amounts to 5 mV and becomes worse for larger currents and/or access resistances. In voltage-jump experiments with large currents and fast kinetics the two kinds of errors described result in a complex dynamic error that renders measurements often not interpretable. Most amplifiers provide an access (series) resistance compensation that compensates both kinds of errors based on an estimate of C_m and R_a. Since the compensation involves positive feedback elements it increases the noise and is prone to oscillations. Care must therefore be taken in their application (see [28]).

Similar to the oocyte system cell-free patches allow a much better voltage-clamp and also faster solution changes. However, because most cells are quite small pipettes can not be as big as for *Xenopus* oocytes rendering "macroscopic" recordings more difficult to achieve in excised patches.

3.3 Leak and capacity subtraction

In heterologous expression systems unwanted currents can be either true leak caused by the recording electrodes or endogenous currents. These have to be carefully avoided using appropriate solutions. The subtraction of currents remaining after application of a specific blocker, if available, at a saturating concentration is a very good but often tedious method. For ligand gated channels the subtraction of currents at zero concentration of ligand is obviously a good method, because the spontaneous open probability is very small for most ligand activated channels. For voltage-gated channels studied by step-protocols the responses are additionally distorted by the capacitive transients. These can be assumed to be linear, meaning that their size is proportional to the voltage step but independent from the voltage from which the pulse is delivered. Thus smaller steps applied in a voltage range where channels are closed or steps to the reversal potential can be used to subtract capacitive transients after appropriate scaling (see for example [29,30]).

4. Macroscopic recordings

In the following sections it is assumed that the ion channel of interest is expressed in a heterologous system and represents the major contribution to the total membrane conductance. The methodologies to extract various biophysical parameters that are useful for a characterization of ion channels are explained.

Single channel measurements, if recorded at a sufficient bandwidth, contain in principle more information than macroscopic ensemble measurements. However, they are technically more demanding, the recordings and analysis and single channel currents are small for many ion channels rendering their analysis impossible. In addition, fast kinetics are difficult to measure at the single channel level because of the lower signal to noise ratio that has to be compensated by heavier filtering. Thus, for many applications

macroscopic recordings represent the only practical approach. The most important relation regarding macroscopic currents is given by

$$I = N * i * p \qquad \text{(Eq. 1)}$$

that expresses the total current, I, through a homogenous population of N independent channels. A basic assumption is that the channel under investigation possesses a single open state with current level i, and without subconductance states. Of course this is an oversimplification for many channels. But not making this assumption renders a practical interpretation of macroscopic currents almost impossible, because it is very hard to tease apart different conductance levels of a single channel from macroscopic recordings. The parameter p represents the open probability of the channel, that is the time- and/or voltage- and/or ligand-dependent probability of the channel to be in a conducting state with an associated current, i. The single parameter p in Eq. (1) summarizes the combined action of all gates of the channels. Often it is useful to think of the gates as independent devices. For example the voltage-gated Na^+ channel of Hodgkin and Huxley has 3 m-gates and one h-gate, all independent from each other such that the parameter p is equivalent to

$$p = m^3 h$$

While the independence of different gates is seldom realistic, it is very useful conceptually. Eq. (1) incarnates one of the dogmas of ion channel biophysics: permeation through the open channel – characterized by the parameter, i – is independent of channel gating – characterized by the parameter, p. This is a very useful conceptual distinction, although in real life it breaks down immediately: the occupancy of the pore by permeating ions generally stabilizes the protein structure and thereby influences gating. However, such effects are generally relatively small with some exceptions. For example in CLC type Cl^--channels permeation and gating are strongly coupled [31,32]. On the other hand, gating has practically no influence on permeation through the open pore, because, by definition

"open" implies an open gate. Any influence of closed gates on ion occupancy of pore binding sites vanishes rapidly after opening of the gate because the two processes occur on vastly different time scales. This assumption becomes questionable only if a rapid "flicker type" gate is present that opens and closes on a time scale more similar to that of ion conduction. For example in KvLQT1 (KCNQ1) K^+ channels a rapid flicker type gate seems to be present that leads to drastic effects of Rb^+ ions on the macroscopic current amplitude [33]. In this case it is difficult to distinguish between an effect of Rb^+ on permeation or gating because the concept of a "gate" becomes questionable.

4.1 Analysis of pore properties - permeation

Two basic parameters are important when considering permeation properties. One is ion selectivity, while the other is conductance. Ion selectivity is the ability to favor one ion compared to another and is expressed as the "permeability" ratio of the two ions, for example p_K/p_{Na} for potassium and sodium. It is, in practice, determined from the reversal potential measured in mixtures of the two ions. The most simple situation is when the ions are present at equal concentrations, one on one side of the membrane, the other on the other side, so called bi-ionic conditions. We consider the example of a cationic channel measured with 150 mM NaCl intracellular and 150 mM KCl extracellular. Then the reversal potential, E_{rev}, is given by

$$E_{rev} = RT/(zF)\ \ln(p_K/p_{Na}) \qquad \text{(Eq. 2)}$$

where R is the gas constant, T the absolute temperature, F the Faraday constant, z the valence ($z=1$ for the example above), and $\ln(.)$ the natural logarithm. At room temperature the factor RT/F amounts to ~25 mV, a value that is very useful to remember for electrophysiologists. Inverting Eq. (2) yields

$$p_K/p_{Na} = e^{zFErev/(RT)}$$

Thus, for example, E_{rev} = 25 mV indicates an e-fold higher permeability of K^+ versus Na^+ (e ~ 2.718). Bi-ionic conditions are preferable but can often not easily be achieved in experimental systems. For example in TEV recordings from oocytes the intracellular solution can not be changed. In this case, the *difference* of the reversal potential that arises by changing from one extracellular solution to another is measured. To obtain a permeability ratio, the Goldman-Hodgkin-Katz equation is used

$$E_{rev} = RT/F \ln((p_K[K]_{ext} + p_{Na}[Na]_{ext}) / (p_K[K]_{int} + p_{Na}[Na]_{int})) \quad \text{(Eq. 3)}$$

where $[K]_{ext}$ is the extracellular K^+ concentration and similar for Na^+ (for anions the sign of the reversal potential has to be inverted). We consider the case that the extracellular concentrations of Na^+ and K^+ are changed from $[Na]_0$ to $[Na]_1$ and from $[K]_0$ to $[K]_1$, respectively, and assume that the measured reversal potential changes from E_0 to E_1. From Eq. (3) follows that the permeability ratio is given by

$$p_K/p_{Na} = ([Na]_1 - [Na]_0 e^{\phi}) / ([K]_0 e^{\phi} - [K]_1)$$

where $\phi = F(E_1-E_0)/(RT) \sim (E_1-E_0)/(25\ mV)$. The assumption is that the intracellular concentrations do not change. When ions of different valence are compared (for example Na^+ and Cl^- or Na^+ and Ca^{2+}) the equations change slightly [1] but the basic type of measurement remains the same.

One important and often overlooked problem of reversal potential measurements is the presence of liquid junction potentials that invariably arise when a solution is exchanged for another. The liquid junction potential is caused by the different mobility of different ions and is most pronounced when small inorganic mobile ions (for example Na^+, Cl^-) are exchanged by large organic quite immobile ions (for example $NMDG^+$, $gluconate^-$). See [34] for how to determine and correct for liquid junction potentials. When the Cl^- concentration is changed care must be taken because most reference electrodes are Ag/AgCl electrodes that must be shielded from the solution exchange for example by agar bridges.

It may be difficult to determine the reversal potential because the current flowing through the channel is small such that endogenous background conductances or a leak conductance dominate the effective reversal potential. One reason for this might be that the gates are closed at the expected reversal potential. This is especially a problem for voltage-gated channels. In this case so-called tail-current analysis can be applied to determine the reversal potential – and in fact the shape of the single channel current-voltage relationship as illustrated in Fig. 2.

INSERT FIGURE 2 HERE

The currents shown in Fig. 2C were simulated based on the two-state scheme shown in Fig. 2A using the pulse-protocol illustrated in Fig. 2B. Opening and closing rate constants are exponentially voltage-dependent such that the channel closes at negative voltages and opens maximally at positive voltages. The channel was assumed to have a linear single-channel current-voltage relationship (i-V) with an imposed reversal potential of E_{rev} = -70 mV. However, from the steady state current-voltage relationship, obtained at the end of the variable pulse (see box in Fig. 2C, squares in Fig. 2D), the reversal potential cannot be obtained, because the open probability is too low. In contrast, the initial current, "immediately" after the end of the activating voltage-step (arrow in Fig. 2C), is measurable at these negative voltage. This "instantaneous tail current" and the resulting instantaneous current-voltage relationship (Fig. 2D, circles) reflect the shape of the single channel current-voltage relationship. This can be seen from the equation

$$I_{tail}(V_t) = N\, p_{end}\, i(V_t) \qquad \text{(Eq. 4)}$$

where I_{tail} is the instantaneous current at the tail-voltage, V_t, p_{end} is the open-probability at the end of the activating prepulse, and $i(V_t)$ is the single channel current at V_t. It is assumed that the open probability immediately after the voltage-step remains at the value

it had at the end of the prepulse (p_{end}). Then, the factor $N * p_{end}$ is independent of the tail voltage, and $I_{tail}(V_t)$ is proportional to $i(V_t)$. If the purpose is only to determine the reversal potential it is not very important to get exactly the initial current, and an average over a short stretch of currents relatively briefly after the voltage jump can be calculated. For measuring the exact shape of the single channel i-V, care must be taken to determine the "correct" initial value. This may be complicated if the deactivation is fast and the voltage jump is associated with a large capacity transient. In this case the time course of the deactivating current (after the capacity transient) is fitted by a suitable function (for example an exponential function) that is then back-extrapolated to time "zero".

Also the determination of the permeability of a blocking ion can be difficult. For example the muscle Cl^- channel CLC-1 is blocked by iodide while iodide has a significant permeability with a permeability ratio of $P_I/P_{Cl} \sim 0.2$. But if extracellular Cl^- is completely exchanged by iodide CLC-1 is totally blocked and the reversal potential is dominated by endogenous background conductances resulting in a wrong estimate of P_I/P_{Cl}. The problem can be solved by exchanging extracellular Cl^- only partially by iodide (for example change from 100 mM Cl^- to a solution containing 20 mM Cl^- and 80 mM iodide) leaving enough Cl^- to allow for a significant conductance. Eq. (3) can be used again to quantify the permeability ratio.

4.2 Analysis of fast voltage-dependent block – the Woodhull model

Tail current analysis is useful to analyze voltage-dependent block by fast blockers. A commonly used model to describe voltage-dependent block is the Woodhull model [1,35]. In this model it is assumed that the charged blocking particle enters the channel pore to a certain distance, and senses therefore part of the transmembrane electric field. Block is quantified by

$$\frac{I(c)}{I(0)} = \frac{1}{1 + \frac{c}{K_D(0)} \exp(z\delta VF/(RT))} \qquad \text{(Eq. 5)}$$

Here $I(c)$ is the current in presence of blocker at concentration c, $K_D(0)$ is the dissociation constant at zero voltage, z the valence of the blocking ion and δ the "electrical" distance of the binding site from the bulk solution, that stands for the fraction of the electric field from the bulk solution to the binding site. Eq. (5) describes simultaneously the concentration and the voltage-dependence of block with just two parameters, $K_D(0)$ and δ (see Fig. 3). Another way to describe the Woodhull-model is in terms of an exponentially voltage-dependent dissociation constant (Fig. 3C). The simplicity of the Woodhull-model makes it attractive and it is often a good initial model. Several assumptions are, however, seldom truly satisfied. Firstly, "blocking" ions are often permeable to some extent and may “punch through” at large voltages. Also, almost all ion channels have multi ion pores in which the ions interact. A blocking ion could displace a permeable ion present at the blocking site within the pore. Such effects add to the intrinsic voltage dependence of block (described by δ) and complicate the picture. The incorporation of such features into mechanistic models is beyond the scope of this chapter. See [1] for a comprehensive description of blocking mechanisms.

INSERT FIGURE 3 HERE

4.3 Information on gating properties from macroscopic measurements

Macroscopic currents can be used to obtain an estimate about the open-probability. According to Eq. (1)

$$I = N * i * p \qquad \text{(Eq. 1)}$$

the macroscopic current is proportional to the open probability, p, but further information or assumptions about the number of channels, N, and the single-channel current, i, are necessary to estimate p from the measured current, I. The number of channels can be assumed to be constant in a typical experiment, as a long as its duration is relatively short and no particular maneuvers are undertaken to enhance or decrease protein turnover. Some ion channels can be drastically affected by co-expression and acute manipulation of co-expressed or endogenous regulating proteins, like the ubiquitin-protein ligase Nedd4 [36]. The number of channels can also be non-specifically affected by agents that lead to a general retrieval of plasma-membrane. For example treating *Xenopus* oocytes with phorbol esters, activators of protein kinase C, leads to an unspecific reduction of expressed conductances via a reduction of the plasma membrane surface [37]. Nevertheless, in most cases, *N* can be regarded as fixed. If measurements are performed at a fixed voltage, as in the case of ligand activated channels or in "isochronous tail-current" measurements for voltage-gated channels (see below) also the single channel current, i, is fixed. Otherwise, the shape of the single-channel current-voltage relationship (i-V) has to be taken into account. For the purpose of extracting information about the open probability, the i-V is parameterized in a phenomenological manner, without necessarily interpreting the corresponding parameters mechanistically. In the absence of direct information the i-V is often assumed to be linear

$$i(V) = \gamma(V - E_{rev})$$

with a single-channel conductance, γ, and a reversal potential, E_{rev}. This assumption is particularly adequate if the reversal potential is relatively close to 0 mV, because in this case the intrinsic "Goldman"-rectification [38] has little influence on the shape of the *i-V*. If the reversal potential is far from zero, and if the channel is highly selective for one ion species present in the solutions, the Goldman-Hodgkin-Katz equation is more adequate to

describe the i-V because it takes the concentrations of the permeable ion on the two sides of the membrane into account [1]:

$$i(V) = K\phi \frac{\exp(z(\phi - \phi_r)) - 1}{\exp(z\phi) - 1} \qquad \text{(Eq. 6)}$$

where K is a constant depending on the ionic concentrations, $\phi = VF/(RT)$ and $\phi_r = E_{rev}F/(RT)$. The non-linear shape of the Goldman current-voltage relationship is illustrated in Fig. 4 for a monovalent cation with a reversal potential of -60 mV. It is also not uncommon that some voltage-dependent block or strong rectification is present that has to be taken into account for the description of the i-V. Such a block can be phenomenologically described by a factor that is inspired from the Woodhull model. For a Goldman-type rectification with additional block the i-V is described by

$$i(V) = K\phi \frac{\exp(z(\phi - \phi_r)) - 1}{\exp(z\phi) - 1} \frac{1}{1 + \exp((V - V_1)/V_2)} \qquad \text{(Eq. 7)}$$

where V_1 and V_2 are empirical parameters describing the block; an example is shown in Fig. 4 (dashed line).

INSERT FIGURE 4 HERE

4.3.1 Equilibrium properties - voltage-gated channels

Two types of pulse protocols are most often used to extract the overall-open probability from macroscopic measurements. They are illustrated in Fig. 5, together with simulated currents based on the 2-state scheme of Fig. 2. In the direct pulse protocol (Fig. 5A, B) pulses are delivered to various potentials and the maximum current during the pulse is plotted versus voltage (Fig. 5C, squares). Usually, the open-probability of voltage-gated channels is parameterized with a Boltzmann distribution, here written in two different versions

$$p_{open} = \frac{1}{1+\exp((V_{1/2} - V)/k)} = \frac{1}{1+\exp(z_g (V_{1/2} - V)F/(RT))} \qquad \text{(Eq. 8)}$$

In both forms the voltage of half-maximal activation, $V_{1/2}$, describes the voltage at which $p_{open} = 0.5$. The steepness of the voltage-dependence is either described by the so-called "slope-factor", k (in mV), or the "apparent gating valence" z_g (dimensionless). These two quantities are inversely related by

$$k = \frac{RT}{z_g F}$$

INSERT FIGURE 5 HERE

The Boltzmann equation derives from the statistical Boltzmann equilibrium that relates the ratio of the probability to be in one of two microscopic states, O and C, that differ in free energy by a certain amount ΔG:

$$\frac{p_O}{p_C} = \exp(-\Delta G/(RT))$$

The Boltzmann distribution of voltage-gated channels (Eq. 8) stems from a simple model for voltage-gated channels that assumes that the free energy difference between the open and the closed state is additively composed of an electrical term, determined by the electrical charge, denoted by Q_C and Q_O, respectively, and a purely chemical term, ΔG_0, such that ΔG is given by

$$\Delta G = \Delta G_0 + V(Q_O - Q_C) = \Delta G_0 + V z_g F$$

where z_g is the apparent gating valence. The larger the charge-difference between closed and open state is, the more sensitive to voltage is the channel, and the steeper the $p_{open}(V)$-curve.

To extract the gating component (p) from the permeation component (i) for currents obtained from the "direct" I-V (Fig. 5C, squares) the I-V is fitted by the product of the i-V term and the Boltzmann-term:

$$I(V) = K\phi \frac{\exp(z(\phi - \phi_r)) - 1}{\exp(z\phi) - 1} \frac{1}{1 + \exp(z_g(V_{1/2} - V)F/(RT))} \qquad \text{(Eq. 9)}$$

Here, in Eq. (9), the Goldman-Hodgkin-Katz equation (Eq. 6) was used for a description of the i-V. The four parameters, K, ϕ_r, $V_{1/2}$, and z_g are obtained from a fit to the macroscopic data, while only the two parameters $V_{1/2}$, and z_g are relevant for gating.

The tail-pulse protocol illustrated in Fig. 5A, B (see arrow) is often called "isochronous tail protocol" because the fixed tail pulse is applied after a fixed amount of time. The initial tail current is a measure of the open-probability at the end of the (variable) pre-pulse (see Eq. (4)). As for the instantaneous I-V (see 4.1) a correct determination of the initial tail-current may be hindered by the capacitive artifact. A careful back-extrapolation of the time course of the tail-current to "time 0" may be necessary to obtain a reliable estimate of the initial tail-current. The tail voltage should be chosen such that the relaxations are well-resolved with the employed voltage-clamp technique.

The resulting initial tail-currents are then plotted versus the pre-pulse voltage (Fig. 5C, circles) and fitted by

$$I(V) = \frac{I_{max}}{1 + \exp(z_g(V_{1/2} - V)F/(RT))} \qquad \text{(Eq. 10)}$$

Here, I_{max}, is the maximal current obtained at saturating voltages. It can be determined by normalization with the measured currents or it can be left as an independent parameter. The latter possibility is particularly adequate if the employed voltage-range is not sufficient to saturate channel gating. In this case the plateau of the Boltzmann-distribution is not reached and currents can not be normalized by the maximally measured value.

Sometimes it happens that currents do not tend to zero at voltages where the channel should close according to Eq. (8). This may be an intrinsic property of the gating mechanism of the channel or may represent an uncompensated leak component. If such a "residual" open probability is an intrinsic property, a description with a Boltzmann-distribution (Eq. 8) is, strictly speaking, not adequate. Nevertheless the shape of the $p_{open}(V)$-curve can often be described phenomenologically by a modified Boltzmann-distribution

$$I(V) = I_{max}\left(p_{min} + \frac{1 - p_{min}}{1 + \exp(z_g (V_{1/2} - V) F/(RT))} \right)$$

where p_{min} describes the minimal open-probability reached at saturating voltages where channels are maximally closed. $V_{1/2}$ is not anymore the voltage at which $p_{open} = 0.5$ but where $p_{open} = p_{min} + 0.5*(1-p_{min})$.

The isochronous tail-current protocol is, in principle, superior to the direct I-V because it is not influenced by the shape of the *i-V*. However, in certain cases a direct method has to be employed. For example, voltage-gated Na^+ channels are governed by two main gating processes of opposite voltage-dependence and one wants to determine separately their respective voltage-dependence. Na^+ channels inactivate with a voltage-dependent time-course after an activating voltage step. The steady state, isochronous tail-current I-V would determine only the "window" current, the region where activation and inactivation gates are both open. To separate the two gates of the Na^+ channel two different protocols are used to assess the voltage-dependence of the activation and the inactivation gate, respectively. The "peak-current" of the direct I-V is generally used as a measure of the activation gate (Fig. 6A, B). This is justified because the time constant of activation is considerably faster than that of inactivation. The inactivation is measured with a two-pulse protocol similar to the isochronous tail-current protocol (Fig. 6C, D).

INSERT FIGURE 6 HERE

4.3.2 Equilibrium properties - ligand gated channels

Conceptually, the determination of equilibrium properties of ligand activated channels is similar to that of voltage-activated channels. The energy driving the conformational change is not supplied by the membrane-voltage but by the chemical energy of ligand binding. Accordingly, the relevant intensive variable is the ligand concentration, here denoted by $[\mathrm{L}]$. However, for ligand activated channels the allosteric action of the ligand is much more evident and explicit than is the voltage for voltage-gated channels [39] (even though most quantitative models of voltage gated channels often have an allosteric character). Thus instead of assuming a scheme of the form

$$U \underset{k_{off}}{\overset{[L]k_{on}}{\rightleftarrows}} O \qquad \text{(Scheme 1)}$$

where binding of a ligand directly opens the channel, the minimal scheme applied for ligand activated channels assumes that binding of the ligand favors opening but does not directly open the channel. This scheme is given by

$$U \underset{k_{off}}{\overset{[L]k_{on}}{\rightleftarrows}} B \underset{\beta}{\overset{\alpha}{\rightleftarrows}} O \qquad \text{(Scheme 2)}$$

with a closed, unliganded state U, a liganded (bound) but closed state, B, and an open state, O [40]. Ligand binding occurs with second-order association rate $\mathrm{k_{on}}$ and dissociation rate $\mathrm{k_{off}}$, while the allosteric transition is described by rate constants α and β.

More complex schemes are necessary to include the possibility that unliganded channels are able to open [39]. Allosteric schemes and equations become even more complex if more than one binding site is present, the usual case in real life. Therefore, mostly for reasons of simplicity, the phenomenological description of ligand-activated channels is often expressed in terms of the Hill equation

$$p_{open} = \frac{p_{\max}}{1 + \left(\frac{K_D}{[L]} \right)^n} \qquad \text{(Eq. 11)}$$

where K_D is the apparent dissociation constant of the binding site(s) and n the Hill-coefficient, an estimate of the number of binding sites [1].

For the simple scheme (2) equilibrium properties can indeed be expressed in the form of Eq. (11)

$$p_{open} = \frac{1}{1 + \frac{1}{r} + \frac{1}{r}\frac{K_D}{[L]}} = \frac{r/(1+r)}{1 + \frac{K_D^*}{[L]}} \qquad \text{(Eq. 12)}$$

where $r=\alpha/\beta$, $K_D=k_{off}/k_{on}$, and the apparent affinity $K_D^* = K_D / (1+r)$. The maximum open-probability is $p_{max} = r / (1+r)=\alpha/(\alpha+\beta)$. Thus, even though the concentration dependence of the macroscopic current strictly follows a 1:1 binding isotherm, the measured apparent affinity can be very different from that of the true affinity of the ligand binding site. K_D^* is always smaller than K_D and only if r is very small ($\alpha<<\beta$) is the apparent affinity equal to the true affinity. But in this case the ligand is not very effective ($p_{max} << 1$). If r is very large, the ligand is very effective ($p_{max} \sim 1$) but the apparent affinity is much higher than the true affinity ($K_D^* << K_D$). Since the absolute open probability is difficult to determine from macroscopic equilibrium measurements alone, additional information is necessary to determine true affinities and ligand efficacies. These can stem from kinetic macroscopic measurements, noise analysis, or single-channel analysis (see below).

A fundamental difference between voltage-gated channels and ligand gated channels is that the latter can be more or less efficiently activated by different types of ligands (for example certain glutamate receptors can be activated also by NMDA), while there is only one stimulus (voltage) for voltage-gated channels. In terms of the simple model shown by scheme (2), quantified by Eq. (12), different ligands have generally a different (true) affinity, and a different efficacy (p_{max}). For ligands that occupy the "same" binding sites the

true number of binding sites is the same. The Hill-coefficient in Eq. (11) may nevertheless be different, since Eq. (11) is an approximate phenomenological description of channel activation. Certain ligands might also counteract the effect of a more potent activator. Furthermore, certain receptors possess different kinds of binding sites. For example certain glutamate receptors need glycine as a co-factor for full activation by glutamate [41]. A good overview over equilibrium properties of ligand gated ion channels with further reference is given by [39].

Many ligand-gated channels exhibit desensitization: currents decrease despite the continuous presence of ligand. The degree and kinetics of desensitization vary wildly between different channel types (see [42] and references therein). This phenomenon is conceptually similar to the "inactivation" of voltage-gated channels. The presence of desensitization complicates the determination of activation properties. Experimentally, the most difficult problem, particularly if desensitization is an issue, is the fast application of the ligand.

4.3.3 Macroscopic kinetics

Channel kinetics can be evoked by a variety of stimuli. Sometimes, biophysical analysis alone is not sufficient to determine the physiological effect in a complex cellular system, as for example a cardiac myocyte, where numerous channel types contribute to the various phases of the action potential. In such cases, a "physiological" stimulation with an action potential wave-form or other stimuli might reveal if, for example a given mutation leads to action potential shortening (see for example [43]). However, such physiological stimuli are not well suited to uncover the underlying mechanistic effect. As outlined in the Introduction, for this purpose clamping the relevant intensive physical parameter (voltage, ligand concentration, temperature, pressure, light intensity, …) to a fixed value and performing jump experiments are more informative. Like practically all kinds of conformational

changes of proteins, current relaxations of a homogenous population of channels induced by a step-wise change of an intensive parameter, can be described by the sum of constant term (the steady-state current, I_∞) and one or more exponential functions

$$I(t) = I_\infty + \sum_{i=1}^{n} a_i \exp(-t/\tau_i) \qquad \text{(Eq. 13)}$$

with amplitudes, a_i, and time constants, τ_i (t is the time after the jump). The kinetics are thus determined by $2n+1$ parameters. The time constants, τ_i, depend only on the actual value of the relevant physical parameter (the voltage or the ligand concentration *after* the jump), while the coefficients, a_i, also depend on the state occupancy *before* the jump. The exponential time dependence is a mathematical consequence from the Markov property of the conformational changes: once the channel undergoes a conformational change it looses "immediately" the memory from what state it arrived (if there is more than one possibility to arrive in a certain state) and it has no memory of how long it is already in a given state. One of the underlying assumptions is, of course, that there exists a finite set of definable, stable "states". Actually, it is more scientific to turn the argument around: the experimental result that relaxation kinetics for most channels can be well described by Eq. (13) (with a reasonably small and reproducible number, n, of components) suggests that the Markov assumption is valid for ion channels. What is a reasonably small number, n? This is indeed a difficult question! In principle, a gating scheme with N states predicts exponential relaxation with $N-1$ components (for example a two-state system has single-exponential kinetics). In practice it is very difficult to reliably fit more than 2 or 3 exponential components. However, gating schemes often require more than 4 states. Indeed it is extremely difficult to define a "correct" gating scheme based on fitting of current relaxations. Often gating schemes that have a large number of states can be simplified with symmetry arguments and the number of free parameters can be reduced. A beautiful example are the Hodgkin-Huxley equations (see [1]), but also recent models of

Shaker K^+ channels have a relatively small number of parameters, despite a large number of states (see [44,45]). Furthermore, current relaxations are often approximately single- or double exponential under certain conditions, even though a full kinetic model requires many states, because most components are negligible. For example the deactivation of Na^+ channels at very negative voltages after a brief activating pulse can be well described by a single exponential even though the general gating involves very many states. Often, kinetics of ion channels are fitted, and time constants are determined phenomenologically without necessarily wanting to define a molecular mechanism of gating. In many circumstances, this is the only practical choice, because the underlying mechanism is too complex to be determined reliably from the measurements. One of the most difficult problems in curve fitting with exponentials is to separate components with time constants that differ less than, let's say 3-fold. Extreme care has to be taken in such cases and reproducibility has to be tested extensively. Often data can be reasonably well described with the sum of two exponentials, even though the "true" mechanism would require at least three. In such cases, the time constants (and relative weights) of the exponential components determined from the double-exponential fit can be almost meaningless. If the true time course is distorted slightly for example by voltage clamp errors (see above) the kinetic analysis becomes even more difficult.

Under certain conditions it is impossible to directly follow the kinetics of a process measuring the ionic current. For example, the channel may be closed quickly by one kind of gate while another gate is changing slowly its status. Another reason that renders impossible a direct measurement might be that the voltage is close to the reversal potential or that a strong block occurs. Also, a large capacitive artifact may obscure fast relaxations [27]. In these cases often so-called “envelope” protocols can be applied as illustrated in Fig. 7 that shows the classical protocol to study the recovery from inactivation

of the voltage-gated Na^+ channel or, completely analogously it illustrates the measurement of the recovery from desensitization of a ligand gated channel.

INSERT FIGURE 7 HERE

It is insightful to explicitly consider the kinetics of the most simple, two state system, because often also more complex schemes can be simplified to it, allowing an easy quantitative description.

$$C \underset{\beta}{\overset{\alpha}{\rightleftharpoons}} O \qquad \text{(Scheme 3)}$$

Opening occurs with rate-constant α, closing with rate constant β. These rate constants depend on the intensive physical parameters (voltage, ligand concentration, …). The equilibrium open probability is

$$p_\infty = \frac{\alpha}{\alpha + \beta}$$

while the relaxation time constant is given by

$$\tau = \frac{1}{\alpha + \beta}$$

Knowing, both p_∞ and τ allows the determination of α and β:

$$\alpha = p_\infty / \tau; \;\; \beta = (1 - p_\infty) / \tau$$

Relaxations that start from a given value of open probability, p_0, proceed in time as

$$p(t) = p_\infty + (p_0 - p_\infty)\exp(-t/\tau)$$

The Del Castillo – Katz model for ligand gated channels (scheme 2) can be reduced to an effective 2-state system if the ligand binding/unbinding is much faster than the opening isomerization transition (described by α and β). In this case the receptor is always in equilibrium with the ligand (see [1]):

$$C \underset{\beta}{\overset{\alpha_{eff}}{\rightleftarrows}} O$$ (Scheme 4)

where the effective opening rate is given by

$$\alpha_{eff} = \frac{1}{1+\frac{K_D}{[L]}}\alpha$$

Combining steady state-measurements (Eq. 12) and relaxation measurements with step-changes in ligand concentration allows the determination of all three parameters (K_D, α, β) of the model of scheme (4): for jumps into zero concentration of ligand, the relaxation rate is $\tau^{-1} = \beta$ because $\alpha_{eff} = 0$ for $[L]=0$. For jumps into saturating concentration of ligand the relaxation rate is $\tau^{-1} = \alpha+\beta$ because $\alpha_{eff} = \alpha$ for $[L]>>K_D$. These kinetic experiments provide thus estimates for α and β. From the equilibrium measurements the apparent affinity, K_D^* is determined (Eq. 12) and using the values for α and β the true affinity, K_D, can be calculated from $K_D = K_D^* (1+\alpha/\beta)$. This simple example illustrates how the combined use of equilibrium and kinetic measurements in addition to simplifying assumptions can be used to obtain quantitative information about a molecular mechanism.

4.4 Channel block

All ion channels interact with a variety of smaller molecules (peptides, small organic molecules) that reduce directly or indirectly ion permeation. Such substances are called blockers or inhibitors and are the bread and butter of the pharmaceutical industry interested in ion channel targets. Inhibitors may directly block the pore and physically impede ion flow. I prefer to call such inhibitors actually channel blockers. Otherwise inhibitors may reduce current flow by stabilizing the closed state of a channel gate. In this case the binding site may be far away from the ionic pore. Such inhibitors are often called "gating modifiers". This distinction between these two kind of inhibitors is actually not so

strict. Many pore blockers additionally alter the gating by binding more tightly to one or another gating state (state-dependent block). Such blockers may be useful tools to study the properties of channel [46,47]. Many pore blockers exert a voltage-dependent block, that can often be described by the Woodhull-model (see 4.2). For most practical purposes channel block is quantified by the Hill equation

$$\frac{I([B])}{I(0)} = \frac{1}{1+\left(\frac{[B]}{K_D}\right)^n}$$

that quantifies the ratio of current in the presence of blocker at concentration $[B]$ to the current in its absence with an apparent affinity K_D and the Hill-coefficient, n.

4.5 Non-stationary noise analysis

The opening and closing of ion channels is a random process that renders current registrations "noisy", in particular if few channels are present. The statistical properties of the noise can be used to infer some characteristics of the underlying elementary events. A prerequisite is that the channel-induced noise is significantly above the background noise of the recording system. This condition is for example generally not fulfilled in TEV recordings from *Xenopus* oocytes. The patch clamp technique, on the other hand, is exceptionally well suited for noise analysis. However, background noise may be large if the series resistance in whole cell recordings is highly compensated (see 3.2). For stationary noise analysis the system is recorded for a prolonged time at fixed external conditions (voltage, ligand concentration, …). The power spectrum is then fitted with the sum of Lorentzian functions. While this method can yield important information [48], non-stationary noise analysis if often faster and easier to perform. Under appropriate conditions, each of the elementary parameters of Eq.(1)

$$I = N * i * p \qquad \text{(Eq. 1)}$$

can be determined under the assumption of a single open conductance level. This should be verified with single channel analysis.

INSERT FIGURE 8 HERE

For standard non-stationary noise analysis a step-protocol (that may be a voltage-step or step-wise change in ligand concentration) is applied repeatedly, with enough time passing between individual stimulations assuring identical initial conditions for each step. Each current response, $I_i(t)$, is recorded ($i=1, \ldots, n$) (Fig. 8A). From these recordings the mean can be calculated by

$$< I(t) >= \frac{1}{n}\sum_{i=1}^{n} I_i(t) \qquad \text{(Eq. 14)}$$

This is now a much smoother curve than the individual traces (Fig. 8 B) and because of this it can be written as

$$< I(t) >= Nip(t)$$

where $p(t)$ is the time course of the ("true") open-probability. The variance of the response, $\sigma^2(t)$, for each time point, t, is given by

$$\sigma^2(t) = \frac{1}{n}\sum_{i=1}^{n}(I_i(t) - < I(t) >)^2 \qquad \text{(Eq. 15)}$$

the standard statistical definition (Fig. 8 C). However, the most important "trick" in non-stationary noise analysis is to calculate the variance not as suggested by Eq. (15) but as the squared difference of consecutive records:

$$\sigma^2(t) = \frac{1}{2(n-1)}\sum_{i=1}^{n-1}(I_{i+1}(t) - I_i(t))^2 \qquad \text{(Eq. 16)}$$

(Note the scaling by a factor of 1/2 in Eq. (16)). For a perfectly stable system the results obtained by Eq. (15) and Eq. (16) are identical. However, in reality, small drifts of the total

current amplitude (“run-down”, “run-up”) or of the reversal potential or other parameters are practically unavoidable. These small drifts are well cancelled out using Eq. (16) while they artificially increase the variance when calculated by Eq. (15) and may render the noise analysis meaningless, particularly if the single channel conductance is small [49]. Meaningful results can be obtained even with run-down up to a factor of two or more. Since the variance is obtained from the differences of records also leak currents and capacity transients cancel out (if they are associated with negligible inherent noise). That means that the individual records do not have to be, and should not be, leak-corrected for the application of Eq. (16), at difference to the calculation of the mean (Eq. 14). A nice property of the variance is that independent noise source add independently to it. Thus, total variance is given by

$$\sigma^2_{tot} = \sigma^2_{channel} + \sigma^2_{background}$$

and the background variance can be usually assumed to be independent of voltage. It can thus be determined at a voltage where no ion current flows through the channels (for example at the reversal potential or in the absence of ligand for ligand activated channels or at a voltage where channels are closed for voltage-gated channels). Having determined the variance and the mean it is now possible to proceed with the "variance-mean analysis". For this we use the equality

$$\sigma^2 = Ni^2 p(1-p) \qquad \text{(Eq. 17)}$$

This fundamental equation [48,49] can be understood intuitively: for p=0 the variance is null because no current flows. Also for p=1 (the maximum value it can attain) there is no fluctuation in the current because all channels are permanently open. The largest fluctuations are present for p=0.5 when channels are half open and half closed on average. Note that (Eq. 17) is independent of the kinetics of the fluctuation. However, the bandwidth of the recording system must be sufficiently large to resolve the fastest transitions. Combining Eq. (17) with Eq. (1) yields

$$\sigma^2 = iI - I^2 / N \qquad \text{(Eq. 18)}$$

that relates the two macroscopic quantities, σ^2, and mean current I, in a parabolic function that depends on two parameters, the single channel current i, and the number of channels, N, that can be determined by a least-squares fit (Fig. 8 D). Often not the whole traces are plotted and fitted against each other but they are first binned in an appropriate manner [49] (see Fig. 8 D). The two parameters, i, and N, are best defined if a large interval of p_{open} is covered by the relaxation. If only a very small interval of p_{open} is sampled, the two parameters can not be determined independently: a small variance can be caused by a small number of channels and/or by a small or large p_{open} and vice versa. It may happen that the current excursion in the relaxation is substantial but that p_{open} remains significantly smaller than 0.5. In this case the second term in Eq. (18) is negligible, the relationship is linear, and only the single channel current can be determined. If both, i and N, can be determined the absolute p_{open} during the relaxation can be calculated from

$$p(t) = \frac{I(t)}{Ni}$$

Thus, using a simple experimental protocol (Fig. 8) allows a quite precise determination of fundamental channel parameters, without the necessity of performing single channel analysis.

4.6 Gating current measurements in voltage-gated channels

Another way of obtaining additional information about molecular gating mechanisms is to measure the so-called "gating currents" associated with the molecular re-arrangements of voltage-gated cation channels [50]. These are transient currents, similar to capacitive currents, that reflect the movement of the gating charges within the electric field. Of course, any conformational rearrangement of the channel protein that is associated with a charge redistribution gives rise to "transient" gating currents, even if they do not reflect the

movement of a "voltage-sensor". However, in voltage-gated K^+, Na^+ and Ca^{2+} channels the voltage-sensor movements clearly dominate the gating-currents. In order to resolve gating currents, that are of small magnitude, it is necessary to eliminate the normal ionic currents by applying blockers or by eliminating permeant ions. However, it must be controlled that such maneuvers of completely eliminating ion flow through the pore does not alter significantly the gating process itself, an often difficult task. It is beyond the scope of this chapter to describe the design and the analysis of gating current measurements (see [51] for review). However, I would like to briefly mention a nice experiment that allowed the estimate of the total gating charge of a single voltage gated K^+ channel [52]. The authors determined first the number of channels, N, in an inside out patch using non-stationary noise analysis (see 4.5). Then they replaced intracellular K^+ with TEA^+, a blocker of K^+ channels to eliminate the ionic currents and measured the total gating charge, Q, by integrating the gating currents. The ratio Q/N, the gating charge per channel, was about 12 elementary charges, consistent with more indirect measurements. Another nice result was obtained by Conti and Stühmer [53], who estimated the size of the charge of a single voltage-sensor in Na^+ channels. Voltage-gated cation channels possess four voltage-sensors that move more or less independently from each other. The movement of each sensor produces a spike-like tiny current. The ensemble of many sensors is the random superposition of many such spikes, filtered with at the recording frequency. Non-stationary noise analysis yielded an elementary charge of individual spikes of about 2.3 elementary charges, a very reasonable value.

5. Single-channel analysis

The possibility to observe and analyze the opening and closing of single ion channel molecules marked a revolution in ion channel research and remains one of the few techniques that allow a true single molecule measurement in real time [3,4]. Single

channel recordings can provide a wealth of information and numerous numerical methods for single channel analysis have been developed. For anybody who is seriously interested in single channel analysis the book "Single channel recording" edited by Sakmann and Neher is a must [54]. Here I can only provide a very broad overview of a typical single channel analysis. Recent papers utilizing more advanced techniques are [55,56].

5.1 Amplitude histogram analysis

The first step of a single-channel analysis is usually to construct an amplitude histogram. Already at this point one ever returning aspect of single channel analysis becomes important: adequate filtering. Of course the data should be filtered with a good filter (for example 8-pole Bessel filter) with a cut-off of at least at one half the sample frequency to avoid aliasing [57]. In order to get, at least in principle, as much information as possible the sampling rate must be sufficiently high. It is however useless to acquire data at a low signal-to-noise ratio. A dilemma is sometimes that one would like to see online the data highly filtered in order to get an immediate impression of the quality of the data, but one wants to acquire also at a higher frequency for quantitative offline analysis. One possibility is to divert the signal after a primary anti-alias filter into two separately sampled channels. One signal is acquired after only the first filter, while in the second channel the current signal is subjected to further filtering for immediate inspection. This can be done on an oscilloscope, or, if the acquiring software allows the simultaneous sampling of two channels the highly filtered signal can be acquired as a second input channel and visualized on the computer screen.

INSERT FIGURE 9 HERE

For the construction of the amplitude histogram all sample points that fall in a given "current-bin" are counted resulting in the number of events per bin that are plotted versus the mid-point of the current bin. This is illustrated in Fig. 9. To each current level of the channel (“closed” and “open” in Fig. 9) corresponds a "peak" in the amplitude histogram. The peaks may be not well separated because noise is large (Fig. 9B). In this case the data can be digitally filtered by a Gaussian filter that has various convenient properties [57] (Fig. 9C). If the baseline is not stable the amplitude histogram becomes distorted. Excessive baseline drift can make the single channel analysis very difficult and must be corrected. Several analysis programs are available that allow baseline correction and many other features.

Once an acceptable amplitude histogram has been constructed it is fitted with the sum of Gaussian functions, G_i, one for each peak, i

$$H(I) = \sum_i G_i(I) = \sum_i \frac{a_i}{\sigma_i} \exp\left(-\frac{(I-\mu_i)^2}{2\sigma_i^2} \right) \qquad \text{(Eq. 19)}$$

where each Gaussian function is characterized by a mean μ_i, a width, σ_i, and an amplitude, a_i. The inclusion of the width, σ_i, in the prefactor a_i/σ_i in the Gaussian fit (Eq. 19) facilitates the calculation of the relative area, A_i, that is occupied by each Gaussian component:

$$A_i = 100\% \frac{a_i}{\sum_j a_j}$$

The relative area, A_i, is a measure of the probability to dwell in the conductance state associated with mean μ_i. Often it happens that the membrane patch contains an unknown number, N, of identical channels, leading to equidistant peaks of the amplitude histogram at levels $n*i$ ($n=0, 1, \ldots$), where i is the amplitude of a single channel. Even though the absolute open probability can not easily be determined in such a situation a useful parameter to evaluate effects of drug application or other maneuvers is the so-called

"Np_O", i.e. the product of the (unknown) number of channels and their open probability. From the histogram fit the "Np_O" can be calculated as

$$Np_O = \frac{\sum_{j=0}^{\infty} jA_j}{\sum_{j=0}^{\infty} A_j}$$

where the "areas" A_j are obtained from the Gaussian fits as described above, and A_0 corresponds to the baseline.

5.2 Kinetic single channel analysis

INSERT FIGURE 10 HERE

A comprehensive description of the kinetic analysis of single channel data is beyond the limits of this chapter and only general directions can be given. The strategic decisions that can be taken for kinetic analysis are schematically outlined in Fig. 10. The most direct way of analysis is depicted on the left of the Figure and consists of directly fitting a "hidden Markov model" to the "raw" data [58-60]. A Markov model is a kinetic scheme like those describe above (for example scheme 2) with possibly many states of various conductance levels connected by rate constants. The rate constants and the conductance levels of the various states are the parameters fitted in this approach. The model is "hidden" for two reasons. First, several kinetic states may be associated with the same conductance. Transitions among these states are therefore not directly visible. Second, the noise can hide short lived dwell times or low conductance states. One advantage of the hidden Markov model approach is that it takes the noise explicitly into account [59,60]. Algorithmically, for the hidden Markov model the following question is raised: for a given set of parameters (these parameters include the rate constants of the model, the

conductance level of each state, and parameters that describe the noise) what is the probability to observe the currents that have been measured? The parameters of the model and the characteristics of the noise are then adapted to maximize this probability. The calculation of this probability is a formidable task but efficient algorithms have been developed that allow the analysis of quite long data sets. One drawback of the method is that a reasonable kinetic model should *a priori* be known. The method can be applied for example to study the effect of mutations of an ion channel for which a kinetic scheme has been established previously. Another drawback is that the method is kind of a black box with little possibility of visual evaluation to check if the results are "reasonable". A further serious problem may occur if the general properties of the noise are not adequately treated [60]. Thus, while the hidden Markov modeling can be a powerful tool, its use requires some experience and results should be checked with other methods.

INSERT FIGURE 11 HERE

The more traditional methods of analysis do not work directly on the raw data trace but this is first "idealized" (Fig. 11). In the idealization process the events of channel opening and closing are detected either completely automatically or interactively using special purpose computer programs. The noisy raw data trace is thus substituted by the idealized smooth trace (Fig. 11) that can be easily represented as a list with two numbers for each entry in the list: the duration of each dwelling together with the corresponding current level. For idealization one must decide if a current fluctuation represents a transition to another conductance level or if it is just noise. As a criterion most often the 50% level criterion is employed [57]. To apply this criterion, the possible conductance levels are estimated first by the fitting of the amplitude histogram (see above). In addition, events are only accepted if they are of a minimal length. For a reliable assignment of the transitions data have to be

filtered usually more than for the hidden Markov approach, at least if the signal to noise level is low. The basic problem in the idealization process is that short events are easily missed (the missed-events problem) but short events can also be artifactually introduced if noise is excessive. The problem is double: missing a short closure not only leads to the loss of a closed event but it also lengthens the opening time of the event during which the closure occurred. Similarly, the artifactual introduction of a short closure not only alters the closed times but also shortens, and divides into two the underlying opening. To deal with this problem in generality is not easy. First, a reasonable cut-off is defined such that no events shorter than this are rigorously accepted and the resulting error in the final fitting procedure can then be compensated [56,61]. For simplicity, we ignore here the missed events problem.

The idealized trace can then be analyzed in several ways. A first step is to construct and inspect dwell-time histograms. Several kinds of binning procedures and histograms to construct have been proposed (see for example [62]). In Fig. 11 so-called cumulative dwell time histograms for the two conductance levels are displayed. These histograms can then be fitted with the sum exponential components in order to extract kinetic information from the single channel data.

The construction and fitting of histograms is always a first step in data analysis if little is known about the underlying channel and if one wants obtain an impression about its kinetic behavior, like for example an estimate of the number of open and closed states. Histogram fitting may also provide a purely empirical set of parameters whose variation under the influence of ligands or mutation can be studied. If a good working hypothesis for a kinetic Markov model for the channel is available it may be instead a good idea to fit directly the likelihood of the idealized channel trace. This approach is similar to the hidden Markov approach described above in that the full kinetic information including possible correlations are exploited. The maximum-likelihood fitting overcomes one of the biggest

problems of histogram fitting: it is not clear how the time-constants and coefficients extracted from closed and open time histograms have to be weighted in fitting a concrete Markov scheme. In the maximum-likelihood approach the rate constants defining the Markov scheme are directly optimized [56,61]. Also recordings obtained under different conditions can be fitted simultaneously. This approach thus allows on one hand an objective estimate of physical parameters similar to the hidden Markov fitting. On the other hand the results can be easily judged visually by comparing the predictions for all kinds of dwell-time histograms [56].

6. Concluding remark

This chapter provided a broad overview about the current concepts and methods of analysis of electrophysiological data. Several of the methods are incorporated into the free analysis program written by the author that is available for download at http://www.ge.cnr.it/ICB/conti_moran_pusch/programs-pusch/software-mik.htm.
Here also the simulation program can be found that was used to generate several of the figures.

Acknowledgements

I thank Armando Carpaneto for critically reading the manuscript. The financial support by Telethon Italy (grant GGP04018) and the Italian Research Ministry (FIRB RBAU01PJMS) is gratefully acknowledged.

References

1. Hille, B. *Ion channels of excitable membranes* (Sinauer, Sunderland, Mass., 2001).
2. Hodgkin, A. L. & Huxley, A. F. A quantitative description of membrane current and its application to conduction and excitation in nerve. *J. Physiol.* **117**, 500-544 (1952).
3. Neher, E. & Sakmann, B. Single-channel currents recorded from membrane of denervated frog muscle fibres. *Nature* **260**, 799-802 (1976).
4. Hamill, O. P., Marty, A., Neher, E., Sakmann, B. & Sigworth, F. J. Improved patch-clamp techniques for high-resolution current recording from cells and cell-free membrane patches. *Pflugers. Arch.* **391**, 85-100 (1981).
5. Doyle, D. A. *et al.* The structure of the potassium channel: molecular basis of K^+ conduction and selectivity. *Science* **280**, 69-77 (1998).
6. Jiang, Y. *et al.* The open pore conformation of potassium channels. *Nature* **417**, 523-526 (2002).
7. Dutzler, R., Campbell, E. B., Cadene, M., Chait, B. T. & MacKinnon, R. X-ray structure of a ClC chloride channel at 3.0 Å reveals the molecular basis of anion selectivity. *Nature* **415**, 287-294 (2002).
8. Bernèche, S. & Roux, B. A microscopic view of ion conduction through the K^+ channel. *Proc. Natl. Acad.Sci. U. S. A.* **100**, 8644-8648. Epub 2003 Jul 01. (2003).
9. Stühmer, W. Electrophysiological recording from Xenopus oocytes. *Methods Enzymol.* **207**, 319-339 (1992).
10. Stühmer, W. Electrophysiologic recordings from Xenopus oocytes. *Methods Enzymol.* **293**, 280-300 (1998).
11. Romero, M. F., Kanai, Y., Gunshin, H. & Hediger, M. A. Expression cloning using Xenopus laevis oocytes. *Methods Enzymol.* **296**, 17-52 (1998).

12. Nagel, G., Szellas, T., Riordan, J. R., Friedrich, T. & Hartung, K. Non-specific activation of the epithelial sodium channel by the CFTR chloride channel. *EMBO Rep.* **2**, 249-254 (2001).

13. Stefani, E., Toro, L., Perozo, E. & Bezanilla, F. Gating of Shaker K^+ channels: I. Ionic and gating currents. *Biophys. J.* **66**, 996-1010 (1994).

14. Barish, M. E. A transient calcium-dependent chloride current in the immature Xenopus oocyte. *J. Physiol.* **342**, 309-325 (1983).

15. Hartzell, C., Putzier, I. & Arreola, J. Calcium-activated chloride channels. *Ann. Rev. Physiol.* **67**, 719-758 (2005).

16. Moriarty, T. M. *et al.* Beta gamma subunits of GTP-binding proteins inhibit muscarinic receptor stimulation of phospholipase C. *Proc. Natl. Acad. Sci. U. S. A.* **85**, 8865-8869 (1988).

17. Pusch, M., Steinmeyer, K., Koch, M. C. & Jentsch, T. J. Mutations in dominant human myotonia congenita drastically alter the voltage dependence of the CIC-1 chloride channel. *Neuron* **15**, 1455-1463 (1995).

18. Firsov, D. *et al.* Cell surface expression of the epithelial Na channel and a mutant causing Liddle syndrome: a quantitative approach. *Proc. Natl. Acad. Sci. U. S. A.* **93**, 15370-15375 (1996).

19. Zerangue, N., Schwappach, B., Jan, Y. N. & Jan, L. Y. A new ER trafficking signal regulates the subunit stoichiometry of plasma membrane K(ATP) channels. *Neuron* **22**, 537-548 (1999).

20. Schwake, M., Pusch, M., Kharkovets, T. & Jentsch, T. J. Surface expression and single channel properties of KCNQ2/KCNQ3, M-type K+ channels involved in epilepsy. *J. Biol. Chem.* **275**, 13343-13348 (2000).

21. Hilgemann, D. W. & Lu, C. C. Giant membrane patches: improvements and applications. *Methods Enzymol.* **293**, 267-280 (1998).

22. Maconochie, D. J. & Knight, D. E. A method for making solution changes in the sub-millisecond range at the tip of a patch pipette. *Pflugers. Arch.* **414**, 589-596 (1989).

23. Kaufman, R. J. Overview of vector design for mammalian gene expression. *Methods. Mol. Biol.* **62**, 287-300 (1997).

24. Nolan, G. P. & Shatzman, A. R. Expression vectors and delivery systems. *Curr. Opin. Biotechnol.* **9**, 447-450 (1998).

25. Bennett, P. B. & Guthrie, H. R. Trends in ion channel drug discovery: advances in screening technologies. *Trends Biotechnol.* **21**, 563-569 (2003).

26. Stühmer, W. *et al.* Structural parts involved in activation and inactivation of the sodium channel. *Nature* **339**, 597-603 (1989).

27. Accardi, A. & Pusch, M. Fast and slow gating relaxations in the muscle chloride channel CLC-1. *J. Gen. Physiol.* **116**, 433-444 (2000).

28. Sigworth, F. J. in *Single-channel recording.* (eds. Sakmanmn, B. & Neher, E.) 95-127 (Plenum Press, New York, 1995).

29. Bezanilla, F. & Armstrong, C. Inactivation of the sodium channel. I. Sodium current experiments. *J. Gen. Physiol.* **70**, 549-566 (1977).

30. Saviane, C., Conti, F. & Pusch, M. The muscle chloride channel ClC-1 has a double-barreled appearance that is differentially affected in dominant and recessive myotonia. *J. Gen. Physiol.* **113**, 457-468 (1999).

31. Pusch, M., Ludewig, U., Rehfeldt, A. & Jentsch, T. J. Gating of the voltage-dependent chloride channel CIC-0 by the permeant anion. *Nature* **373**, 527-531 (1995).

32. Chen, T.-Y. Structure and function of CLC channels. *Ann. Rev. Physiol.* **67**, 809-839 (2005).

33. Pusch, M., Bertorello, L. & Conti, F. Gating and flickery block differentially affected by rubidium in homomeric KCNQ1 and heteromeric KCNQ1/KCNE1 potassium channels. *Biophys. J.* **78**, 211-226 (2000).

34. Neher, E. Correction for liquid junction potentials in patch clamp experiments. *Methods Enzymol.* **207**, 123-131 (1992).

35. Woodhull, A. M. Ionic blockage of sodium channels in nerve. *J. Gen. Physiol.* **61**, 687-708 (1973).

36. Staub, O. *et al.* Regulation of stability and function of the epithelial Na^+ channel (ENaC) by ubiquitination. *EMBO J.* **16**, 6325-6336 (1997).

37. Awayda, M. S. Specific and nonspecific effects of protein kinase C on the epithelial Na^+ channel. *J. Gen. Physiol.* **115**, 559-570 (2000).

38. Goldman, D. E. Potential, impedance, and rectification in membranes. *J. Gen. Physiol.* **27**, 37-60 (1943).

39. Krusek, J. Allostery and cooperativity in the interaction of drugs with ionic channel receptors. *Physiol. Res.* **53**, 569-579 (2004).

40. Del Castillo, J. & Katz, B. Interaction at end-plate receptors between different choline derivatives. *Proc. R. Soc. Lond. B. Biol. Sci.* **146**, 369-381 (1957).

41. Clements, J. D. & Westbrook, G. L. Activation kinetics reveal the number of glutamate and glycine binding sites on the N-methyl-D-aspartate receptor. *Neuron* **7**, 605-613 (1991).

42. Changeux, J. P. & Edelstein, S. J. Allosteric receptors after 30 years. *Neuron* **21**, 959-980 (1998).

43. Berecki, G. *et al.* HERG Channel (Dys)function Revealed by Dynamic Action Potential Clamp Technique. *Biophys. J.* **88**, 566-578 (2005).

44. Zagotta, W. N., Hoshi, T. & Aldrich, R. W. Shaker potassium channel gating. III: Evaluation of kinetic models for activation. *J. Gen. Physiol.* **103**, 321-362 (1994).

45. Zheng, J. & Sigworth, F. J. Selectivity Changes during Activation of Mutant Shaker Potassium Channels. *J. Gen. Physiol.* **110**, 101-117 (1997).

46. Koch, E. D., Olivera, B. M., Terlau, H. & Conti, F. The Binding of {kappa}-Conotoxin PVIIA and Fast C-Type Inactivation of Shaker K^+ Channels are Mutually Exclusive. *Biophys. J.* **86**, 191-209 (2004).

47. Pusch, M. *et al.* Mechanism of block of single protopores of the Torpedo chloride channel ClC-0 by 2-(p-chlorophenoxy)butyric acid (CPB). *J. Gen. Physiol.* **118**, 45-62 (2001).

48. Conti, F. Noise analysis and single-channel recordings. *Current Topics in Membranes and Transport* **22**, 371-405 (1984).

49. Heinemann, S. H. & Conti, F. Nonstationary noise analysis and application to patch clamp recordings. *Methods Enzymol.* **207**, 131-148 (1992).

50. Armstrong, C. M. & Bezanilla, F. Currents related to movement of the gating particles of the sodium channels. *Nature* **242**, 459-461 (1973).

51. Bezanilla, F. The voltage sensor in voltage-dependent ion channels. *Physiol. Rev.* **80**, 555-592 (2000).

52. Schoppa, N. E., McCormack, K., Tanouye, M. A. & Sigworth, F. J. The size of gating charge in wild-type and mutant Shaker potassium channels. *Science* **255**, 1712-1715 (1992).

53. Conti, F. & Stühmer, W. Quantal charge redistributions accompanying the structural transitions of sodium channels. *Eur. Biophys. J.* **17**, 53-59 (1989).

54. Sakmann, B. & Neher, E. *Single-channel recording.* (Plenum Press, 1995).

55. Qin, F. Restoration of single-channel currents using the segmental K-means method based on Hidden Markov Modeling. *Biophys. J.* **86**, 1488-1501 (2004).

56. Colquhoun, D., Hatton, C. J. & Hawkes, A. G. The quality of maximum likelihood estimates of ion channel rate constants. *J Physiol (Lond)* **547**, 699-728 (2003).

57. Colquhoun, D. & Sigworth, F. J. in *Single-channel recording.* (eds. Sakmanmn, B. & Neher, E.) 483-585 (Plenum Press, New York, 1995).

58. Chung, S. H., Moore, J. B., Xia, L. G., Premkumar, L. S. & Gage, P. W. Characterization of single channel currents using digital signal processing techniques based on Hidden Markov Models. *Philos. Trans. R. Soc. Lond. B Biol. Sci.* **329**, 265-285 (1990).

59. Qin, F., Auerbach, A. & Sachs, F. Hidden Markov modeling for single channel kinetics with filtering and correlated noise. *Biophys. J.* **79**, 1928-1944 (2000).

60. Venkataramanan, L. & Sigworth, F. J. Applying hidden Markov models to the analysis of single ion channel activity. *Biophys. J.* **82**, 1930-1942 (2002).

61. Qin, F., Auerbach, A. & Sachs, F. Estimating single-channel kinetic parameters from idealized patch-clamp data containing missed events. *Biophys. J.* **70**, 264-280 (1996).

62. Sigworth, F. J. & Sine, S. M. Data transformations for improved display and fitting of single-channel dwell time histograms. *Biophys. J.* **52**, 1047-1054 (1987).

Figure legends

Figure 1. The intracellular series resistance in *Xenopus* oocytes. Current flowing through the interior of the oocyte leads to a voltage drop caused by the finite resistance of the cytoplasm.

Figure 2. Tail current analysis. Macroscopic currents were simulated for the two state scheme shown in A. The reversal potential was -70 mV. From the holding-potential of -80 mV a 0.2 sec prepulse to 60 mV was followed by variable pulses ranging from -140 to 80 mV as illustrated in B. At negative voltages currents deactivate quickly such that the reversal potential can not be reliably obtained from the steady-state currents (squares in D). The initial tail currents (circles in D) faithfully reproduce the linear single-channel current-voltage relationship and allow a precise determination of the reversal potential.

Figure 3. Illustration of the Woodhull model of channel block. A linear single-channel i-V and a zero reversal potential was assumed for the unblocked channel (solid line in A). The parameters of the block were $K_D(0)=1\ mM$ and $z^*\delta = 0.4$. Application of increasing amounts of blocker (0.5, 1, and 5 mM) produces the increasing voltage-dependent block (dashed lines in A). The concentration dependence of block is illustrated in B for different voltages (-100, -30, 30, and +100 mV). The exponential voltage-dependence of the apparent K_D, determined by fitting the curves in B with a simple 1:1 binding curve is illustrated in C.

Figure 4. The Goldman-Hodgkin-Katz equation. The solid line is drawn according to Eq. (6) with $E_{rev} = -60\ mV$. The dashed line is drawn according to Eq. (7) with $E_{rev} = -60\ mV$ and $V_1 = V_2 = 50\ mV$.

Figure 5. Determination of the open probability for voltage gated channels. Currents were simulated according to the 2-state scheme shown in Fig. 2A assuming a reversal potential of 0 mV and applying the pulse protocol shown in A. Steady state currents measured at the end of the variable-voltage pulse (see arrow in B) are plotted in C as squares. The tail currents at the beginning of the constant tail pulse to 60 mV are shown as circles.

Figure 6. Activation and inactivation of voltage-gated sodium channels. Currents were recorded from tsA201 cells transfected with the cardiac sodium channel and measured using the whole cell configuration of the patch clamp technique. In A currents were elicited by 10 ms voltage steps from -80 to 50 mV (see inset). In B the peak currents are plotted versus the test voltage (symbols) superimposed with a fit of the equation

$$I(V) = G_{Na}(V - E_{rev})\frac{1}{1+\exp(z_g(V_{1/2} - V)F/(RT))}$$

as shown by the lines. C shows currents from a different cell evoked by the a two-pulse protocol as shown in the inset. The response to the 100 ms long prepulse to voltages from -120 to -10 mV is not shown. The currents represent the response to the fixed tail pulse to -10 mV that assays channel availability. The peak currents are plotted in D (symbols) together with a fit of Eq. (10). Note that activation (A, B) and inactivation (C, D) have an opposite voltage-dependence.

Figure 7. Envelope protocol to study recovery from inactivation. The pulse protocol is illustrated in A, current traces are shown in B. Currents during the recovery period are not shown. In C the peak current at the final test pulse is plotted versus the recovery time together with a single exponential fit. Currents were simulated with a simplified Hodgkin-Huxley model.

Figure 8. Non-stationary noise analysis. Currents were repeatedly evoked by a test-pulse and individual responses are shown in A (currents were simulated with a simplified Hodgkin-Huxley model). The mean and the variance are shown in B and C, respectively. In D the (binned) variance is plotted versus the respective mean together with a fit of Eq. (18). The horizontal line in D marks the level of the background variance.

Figure 9. Amplitude histogram analysis. Currents were simulated based on a simple 2-state scheme with an open conductance level of 1 pA and an added Gaussian noise of 0.4 pA SD (panel A). The baseline and the open conductance level are indicated by horizontal lines. The noisy trace in A seems to be almost useless. However, the amplitude histogram shown in B shows clearly two peaks at the right amplitudes (0 pA and 1 pA), and the fit with the sum of two Gaussian functions (thick line in B) correctly predicts the amplitude and area of each conductance level. The trace shown in C is strongly filtered and the histogram in D shows two well-separated peaks of correct amplitude and weight. The bin-width used for the histograms was 10 fA.

Figure 10. Flow diagram of strategies for kinetic single channel analysis.

Figure 11. Dwell-time analysis. In A a short stretch of a simulated trace of a two state scheme is shown. In B the corresponding idealized trace is displayed. The cumulative dwell-time histograms shown in C and D are based on a total of 408 events each and represent the relative frequency of events to be longer than a given duration. By definition the cumulative distribution equals 1 for a duration of 0. A single exponential dwell-time distribution is represented by a straight line in the logarithmic scaling of Fig. 11. Other representations of dell-time histograms are probably more common [62] but require a much larger number of events for a satisfactory graphical display.

Figure 1

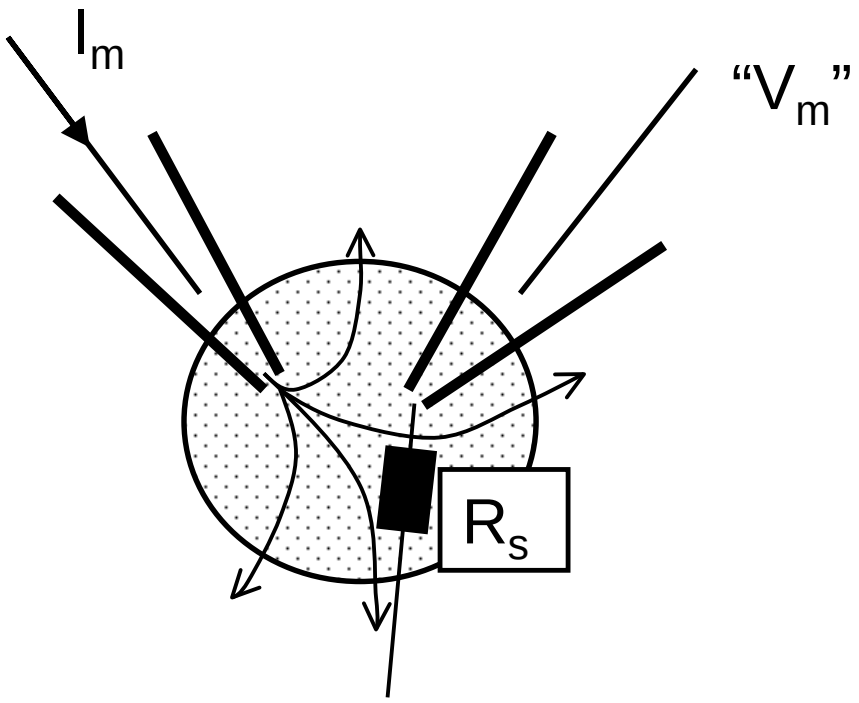

Figure 2

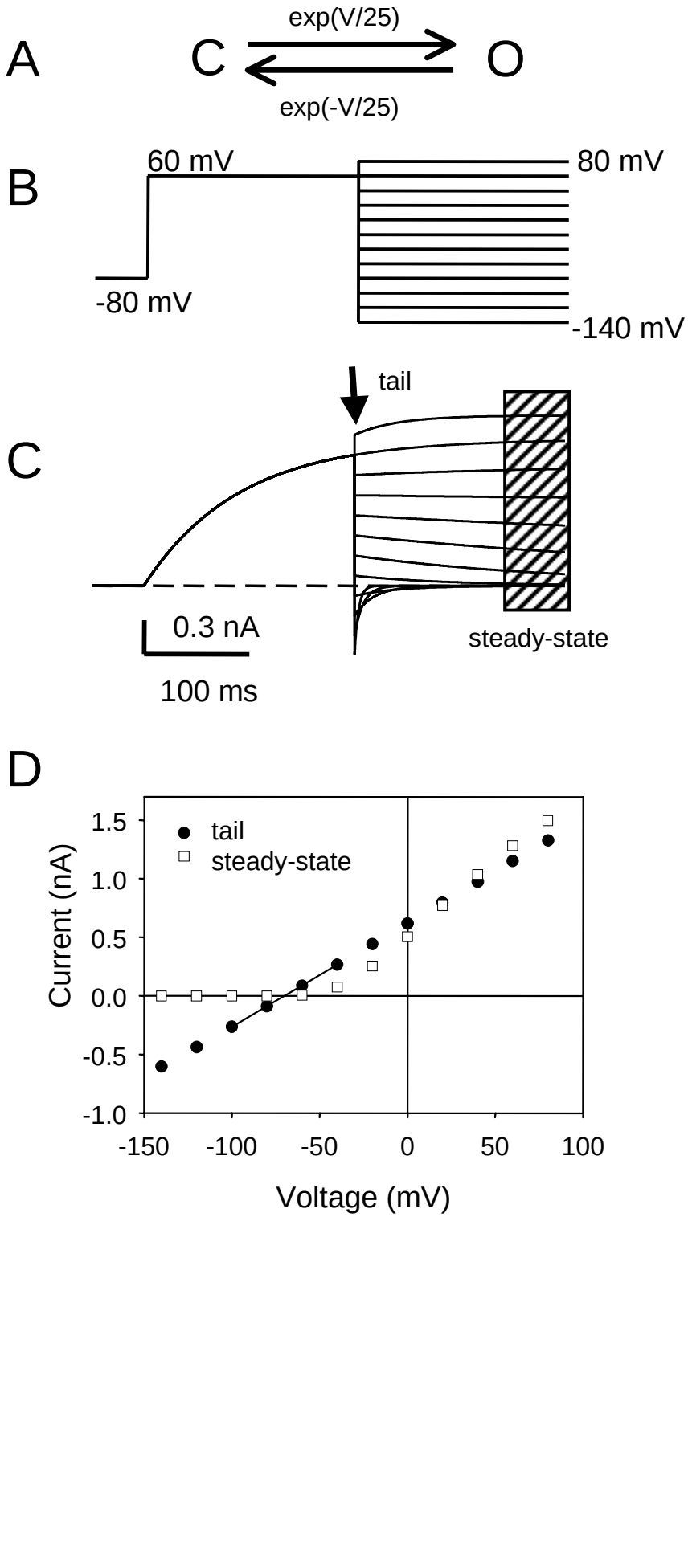
A
exp(V/25)
C
O
exp(-V/25)
B
60 mV
80 mV
-80 mV
-140 mV
C
tail
0.3 nA
steady-state
100 ms
D
tail
steady-state
Current (nA)
1.5
1.0
0.5
0.0
-0.5
-1.0
-150
-100
-50
0
50
100
Voltage (mV)

Figure 3

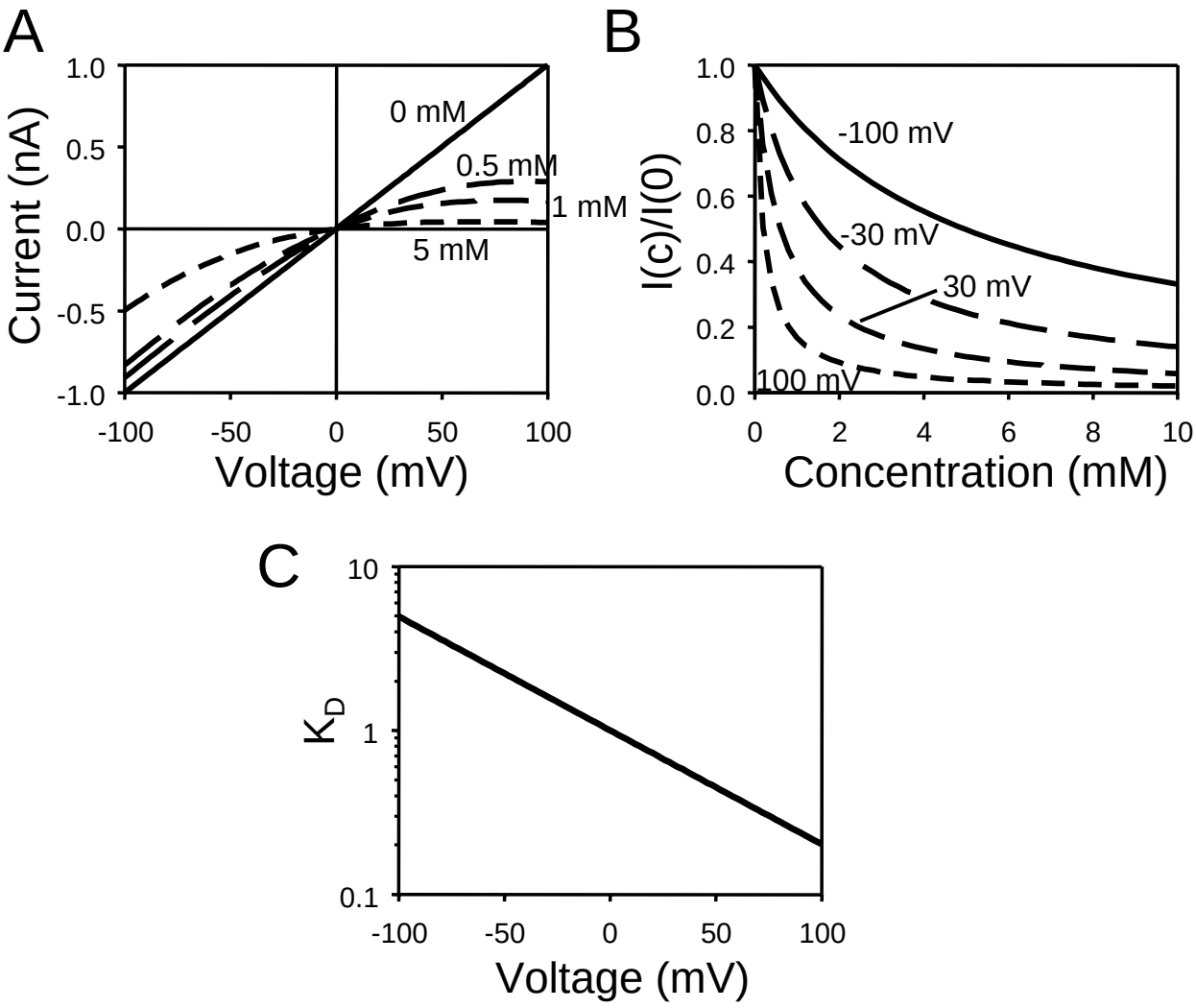
A
Current (nA)
1.0
0.5
0.0
-0.5
-1.0
-100
-50
0
50
100
Voltage (mV)
0 mM
0.5 mM
1 mM
5 mM
B
I(c)/I(0)
1.0
0.8
0.6
0.4
0.2
0.0
0
2
4
6
8
10
Concentration (mM)
-100 mV
-30 mV
30 mV
100 mV
C
K_D
10
1
0.1
-100
-50
0
50
100
Voltage (mV)

Figure 4

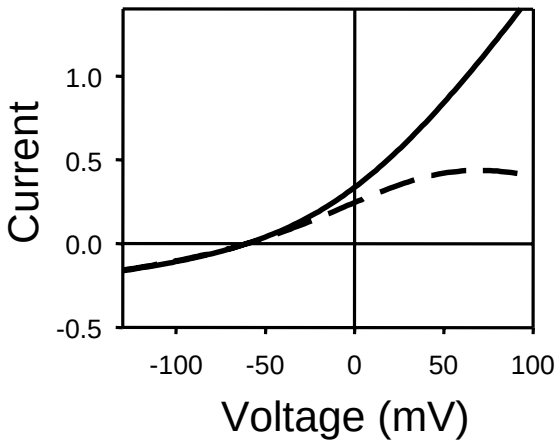

Figure 5

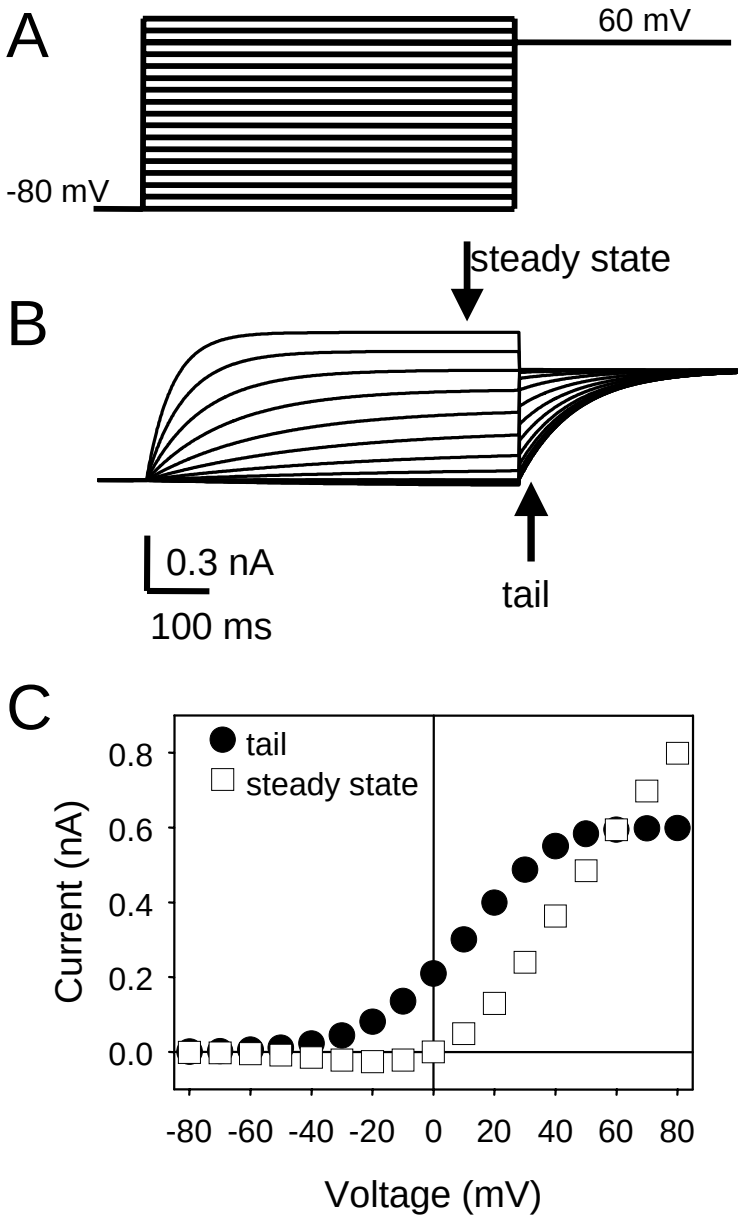
A
60 mV
-80 mV
steady state
B
0.3 nA
100 ms
tail
C
tail
steady state
Current (nA)
0.8
0.6
0.4
0.2
0.0
-80 -60 -40 -20 0 20 40 60 80
Voltage (mV)

Figure 6

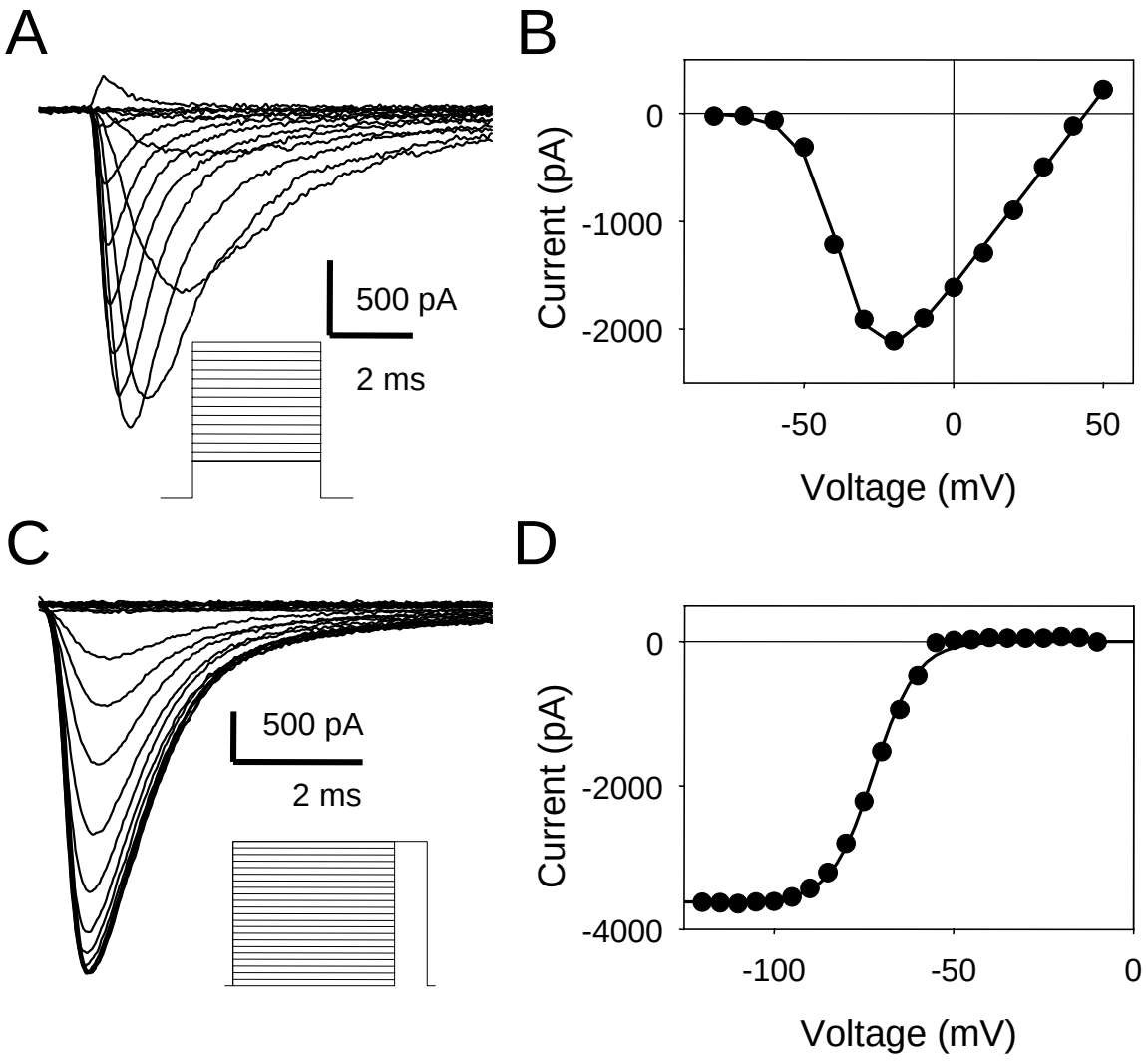
A
500 pA
2 ms
B
0
-1000
-2000
Current (pA)
-50
0
50
Voltage (mV)
C
500 pA
2 ms
D
0
-2000
-4000
Current (pA)
-100
-50
0
Voltage (mV)

Figure 7

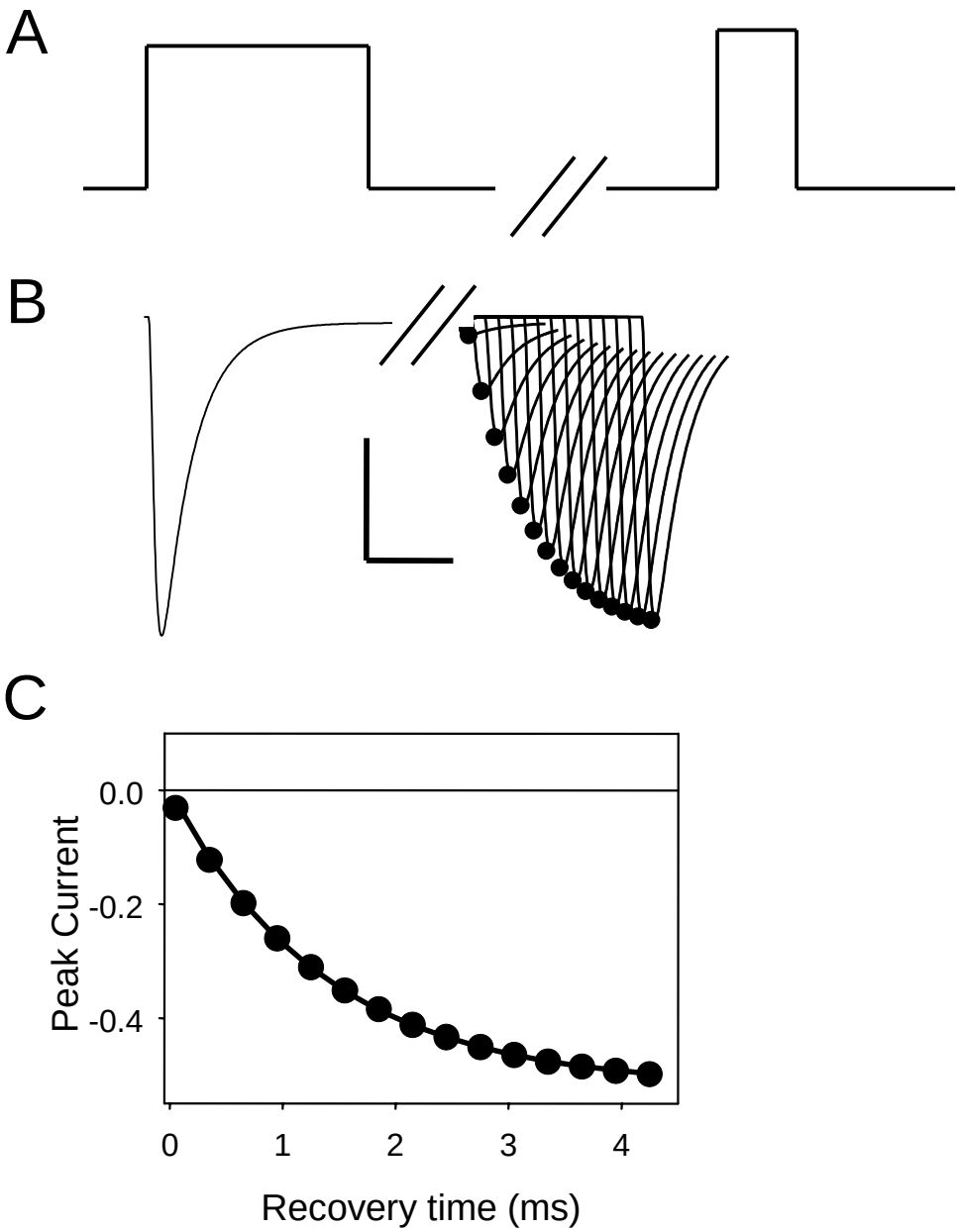

Figure 8

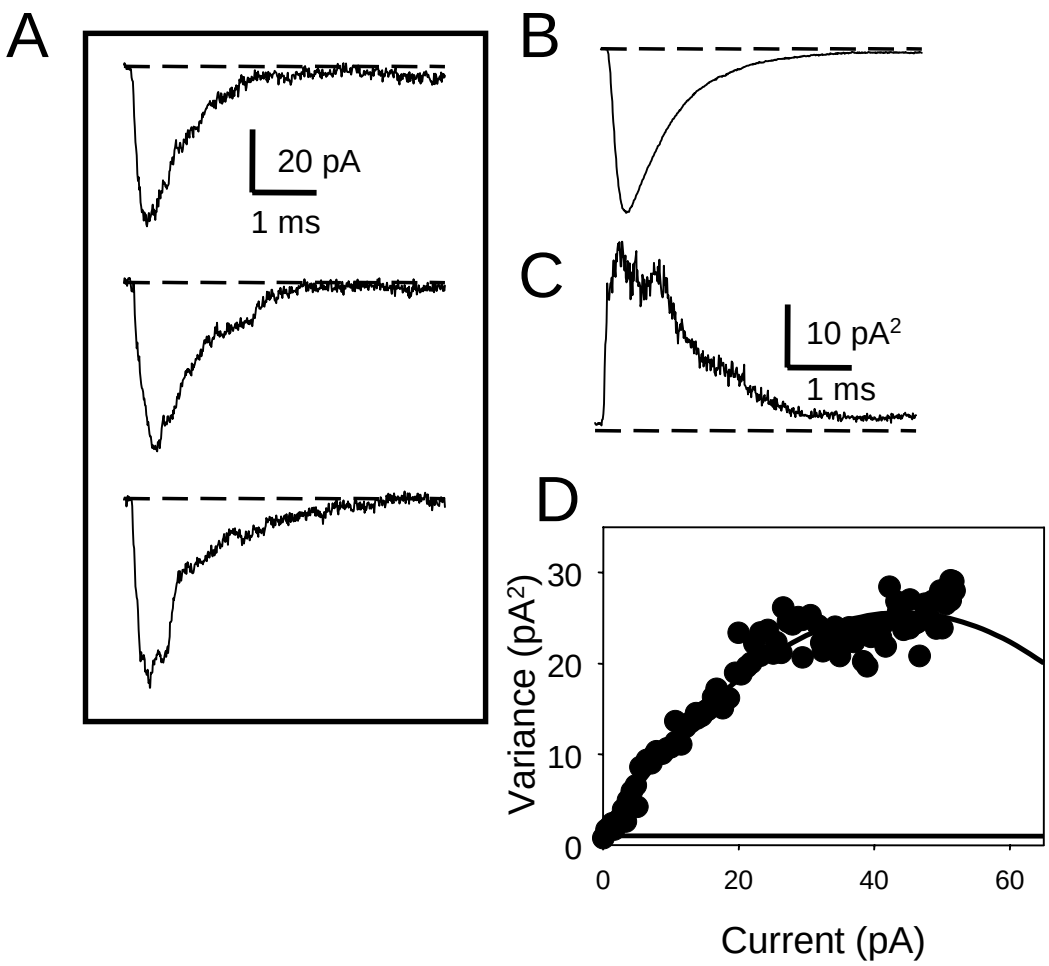
A
20 pA
1 ms
B
C
10 pA2
1 ms
D
Variance (pA2)
30
20
10
0
0
20
40
60
Current (pA)

Figure 9

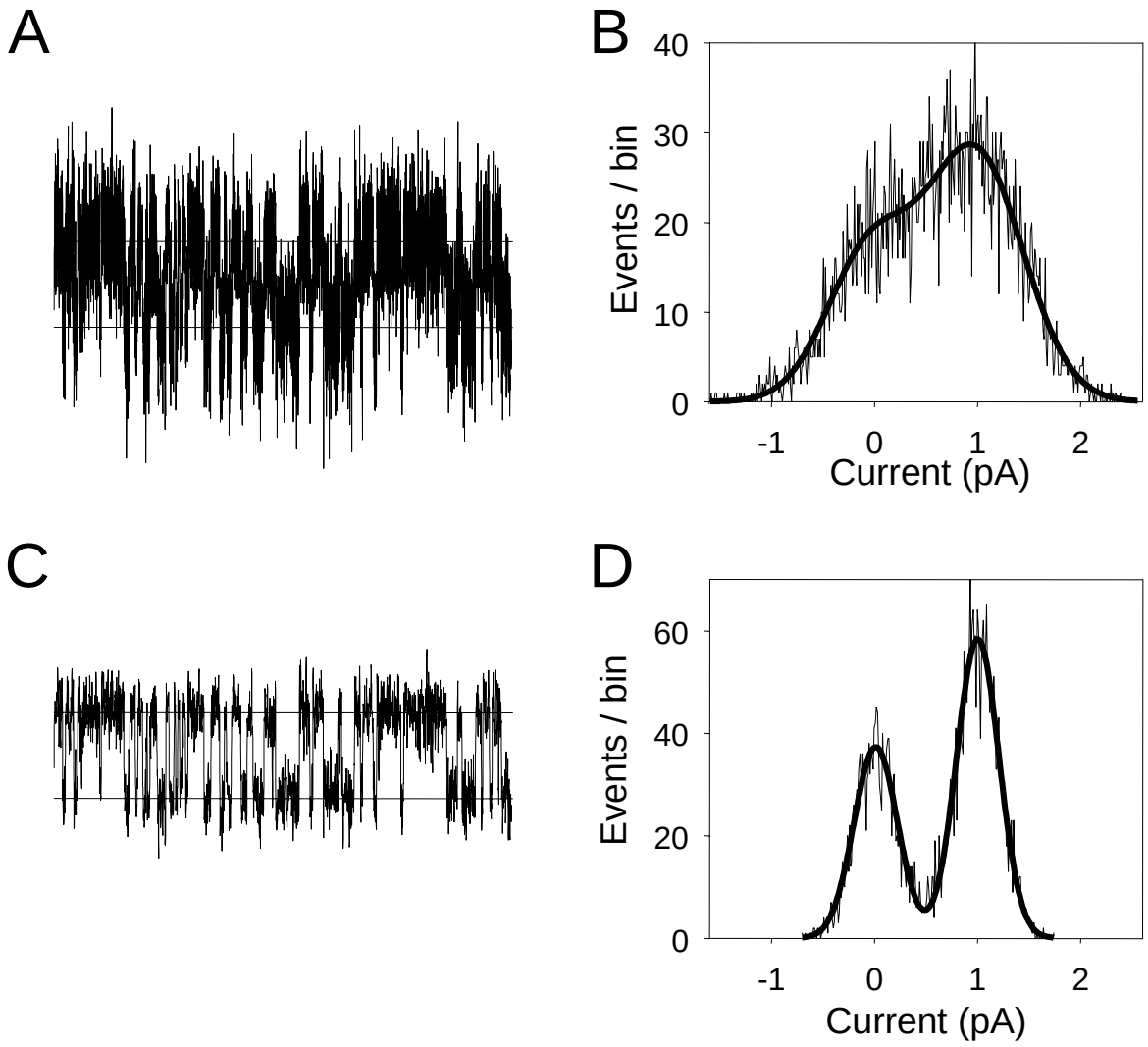
A
B
40
30
20
10
0
Events / bin
-1
0
1
2
Current (pA)
C
D
60
40
20
0
Events / bin
-1
0
1
2
Current (pA)

Figure 10

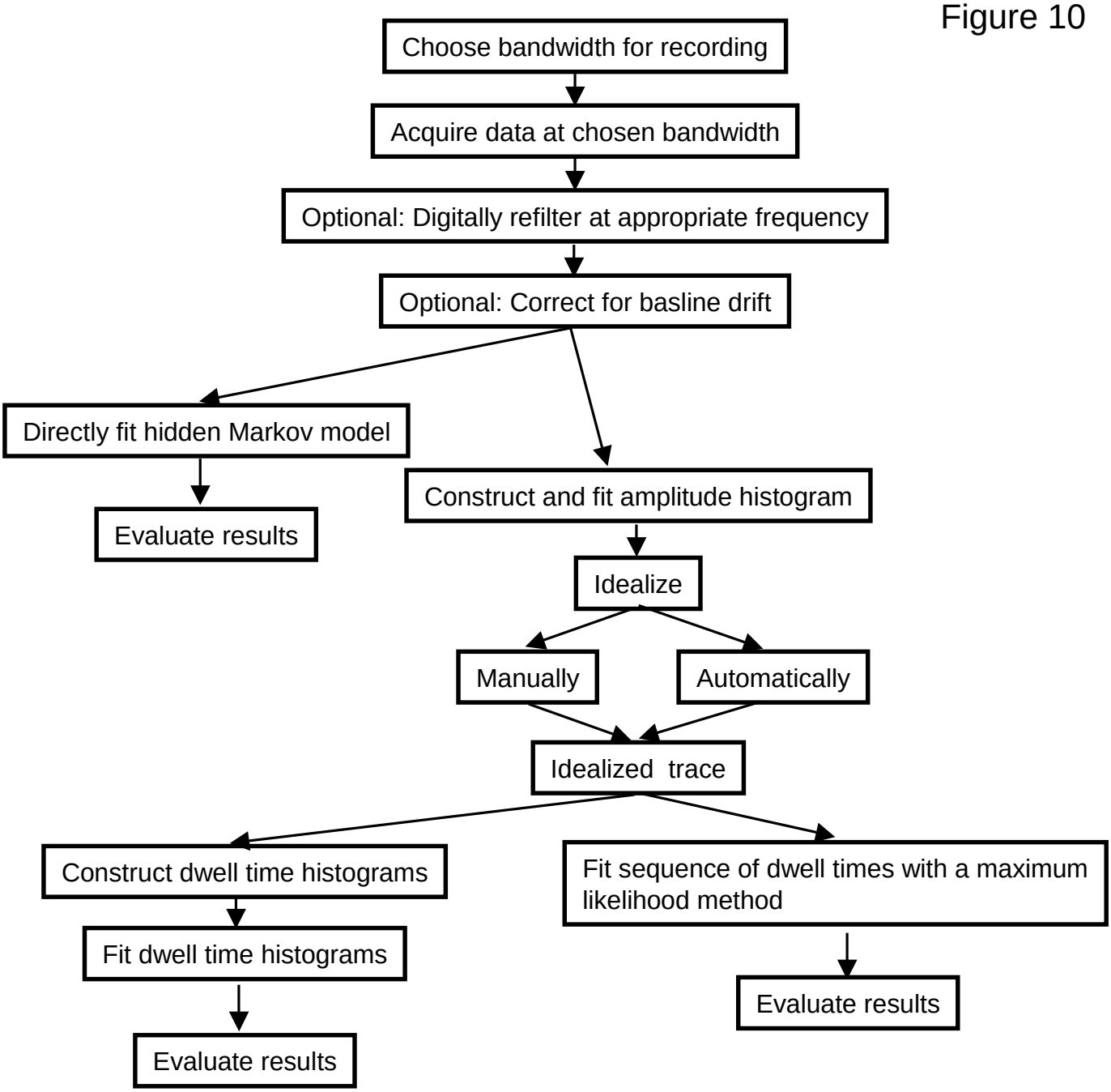
Choose bandwidth for recording
Acquire data at chosen bandwidth
Optional: Digitally refilter at appropriate frequency
Optional: Correct for basline drift
Directly fit hidden Markov model
Evaluate results
Construct and fit amplitude histogram
Idealize
Manually
Automatically
Idealized trace
Construct dwell time histograms
Fit dwell time histograms
Evaluate results
Fit sequence of dwell times with a maximum likelihood method
Evaluate results

Figure 11

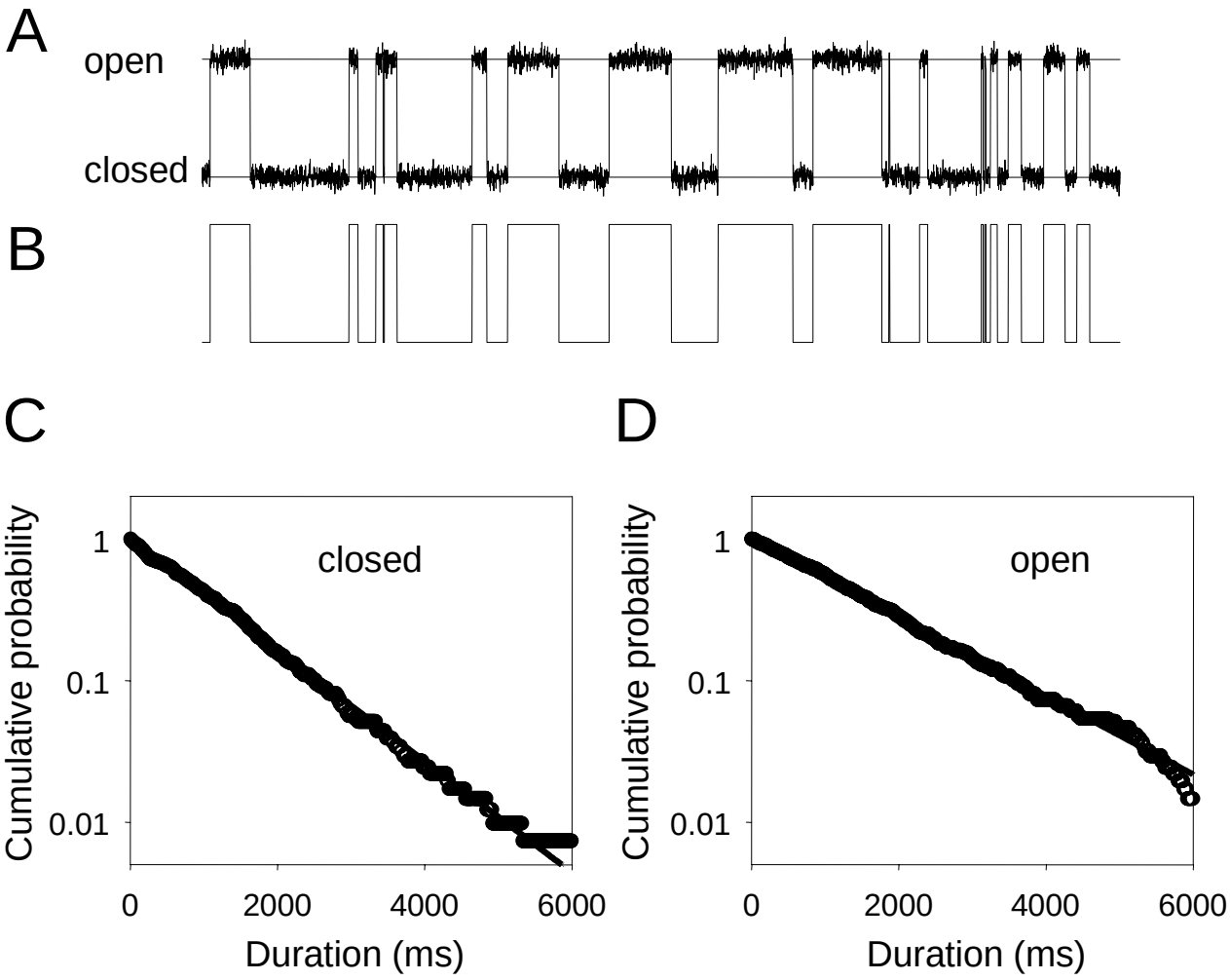
A
open
closed
B
C
Cumulative probability
1
0.1
0.01
closed
0
2000
4000
6000
Duration (ms)
D
Cumulative probability
1
0.1
0.01
open
0
2000
4000
6000
Duration (ms)